

Hydrography of the eastern tropical Pacific: A review

Paul C. Fiedler ^{a,*}, Lynne D. Talley ^b

^a NOAA Fisheries, Southwest Fisheries Science Center, La Jolla, CA 92037, USA

^b Scripps Institution of Oceanography, University of California San Diego, La Jolla, CA 92093, USA

Abstract

Eastern tropical Pacific Ocean waters lie at the eastern end of a basin-wide equatorial current system, between two large subtropical gyres and at the terminus of two eastern boundary currents. Descriptions and interpretations of surface, pycnocline, intermediate and deep waters in the region are reviewed. Spatial and temporal patterns are discussed using (1) maps of surface temperature, salinity, and nutrients (phosphate, silicate, nitrate and nitrite), and thermocline and mixed layer parameters, and (2) meridional and zonal sections of temperature, salinity, potential density, oxygen, and nutrients. These patterns were derived from World Ocean Database observations by an ocean interpolation algorithm: loess-weighted observations were projected onto quadratic functions of spatial coordinates while simultaneously fitting annual and semiannual harmonics and the Southern Oscillation Index to account for interannual variability. Contrasts between the equatorial cold tongue and the eastern Pacific warm pool are evident in all the hydrographic parameters. Annual cycles and ENSO (El Niño-Southern Oscillation) variability are of similar amplitude in the eastern tropical Pacific, however, there are important regional differences in relative variability at these time scales. Unique characteristics of the eastern tropical Pacific are discussed: the strong and shallow pycnocline, the pronounced oxygen minimum layer, and the Costa Rica Dome. This paper is part of a comprehensive review of the oceanography of the eastern tropical Pacific.

© 2006 Elsevier Ltd. All rights reserved.

Keywords: Hydrography; Water masses; Thermocline; Oxygen minimum layer; Mixed layer depth; Tropical oceanography; Eastern tropical Pacific; Costa Rica Dome

1. Introduction

The eastern tropical Pacific Ocean is not defined by a single ocean basin, water mass, current system, or ecosystem. It is a region between the subtropical gyres of the North and South Pacific and contains both the eastern terminus of the equatorial current system of the Pacific (Kessler, 2006) and the eastern Pacific warm pool that forms half of the western hemisphere warm pool straddling Central America (Wang and Enfield, 2001). Eastern boundary currents flow into the region from the north (California Current) and south

* Corresponding author. Tel.: +1 858 546 7016; fax: +1 858 546 7198.
E-mail address: Paul.Fiedler@noaa.gov (P.C. Fiedler).

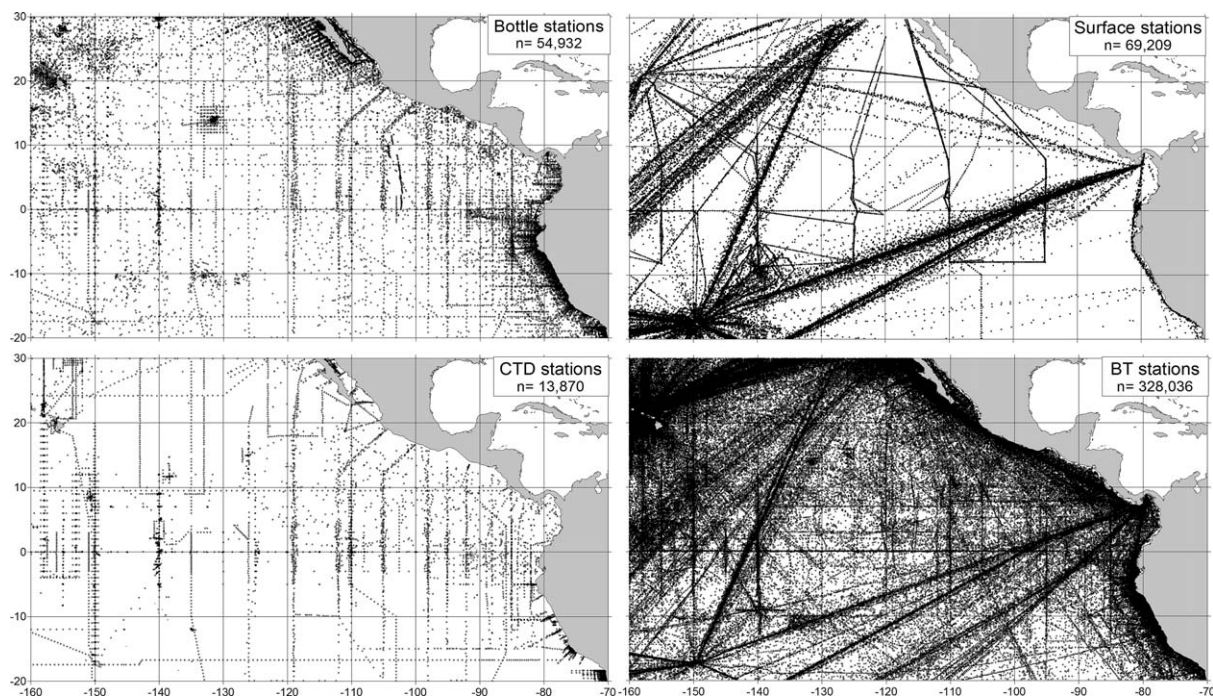


Fig. 1. Locations of 1950–2002 hydrographic stations from World Ocean Database 2001 (WOD01, see [Appendix](#)). CTD, conductivity–temperature–depth profiles. BT (bathythermograph) stations include 164,221 MBTs (mechanical) and 163,815 XBTs (expendable).

(Peru Current). The eastern tropical Pacific is important for its roles in climate variability due to the El Niño–Southern Oscillation, in fish production, and in the global carbon cycle (Fiedler and Lavín, 2006).

This paper reviews descriptions and interpretations of spatial and temporal patterns of surface, pycnocline, intermediate and deep waters in the region. This hydrography is related to physical forcing described in companion reviews of the eastern tropical Pacific atmosphere (Amador et al., 2006) and circulation (Kessler, 2006). Hydrography, in turn, forms a basis for the reviews of physical and biological patterns in this volume. Spatial and temporal patterns are discussed using (1) maps of surface temperature, salinity, and nutrients (phosphate, silicate, nitrate and nitrite), and thermocline and mixed layer parameters, (2) meridional and zonal sections of temperature, salinity, potential density, oxygen, and nutrients and (3) mean profiles illustrating stratification. Maps, sections and profiles are based on CTD (conductivity–temperature–depth), bathythermograph, and bottle data (Fig. 1). Note that the data and methods used to create the hydrographic fields illustrating this review are described in the [Appendix](#). This paper is part of a comprehensive review of the oceanography of the eastern tropical Pacific.

2. Surface waters

General hydrographic features of the eastern tropical Pacific are illustrated by the pattern of mean surface temperature (Figs. 2 and 3). The eastern Pacific warm pool ($>27.5\text{ }^{\circ}\text{C}$) is centered along the coast of southwestern Mexico and Guatemala. Relatively cold surface waters mark the equatorial cold tongue and the eastern boundary current waters along Baja California to the north (California Current) and Ecuador and Peru to the south (Peru Current). The eastern Pacific warm pool is the result of seasonally large net heat flux and weak wind mixing (Wang and Enfield, 2001). This warm pool is connected to the larger and slightly warmer (up to $30\text{ }^{\circ}\text{C}$) Pacific warm pool in the western Pacific by a band of $27\text{ }^{\circ}\text{C}$ water centered along 7°N latitude (see Fig. 6). This warm band marks a thermal equator: the amplitude of the seasonal cycle is low in this warm band, except near the coast of Central America, while quarterly deviations (Fig. 3b) and phases of the annual cycle (Fig. 3c) are opposite to the north and south of the band.

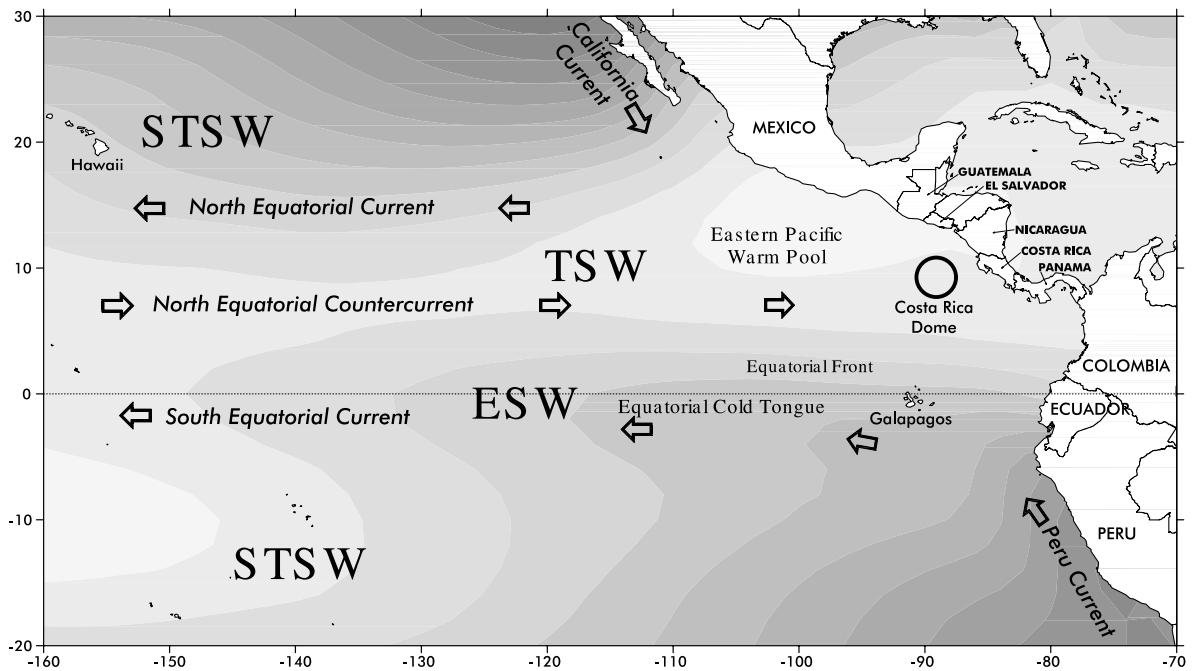


Fig. 2. Schematic diagram of surface water masses and currents in the eastern tropical Pacific Ocean. STSW, Subtropical Surface Water; TSW, Tropical Surface Water; ESW, Equatorial Surface Water. Shading represents mean sea surface temperature (darker = colder; Shea et al., 1992).

The equatorial cold tongue is centered directly on the equator west of 120°W, and slightly south of the equator to the east. Surface water properties here “are determined by seasonal advection of cooler water from the Peru Current and by equatorial upwelling” (Wyrtki, 1966, 1981). Temperature of the cold tongue decreases towards the east as progressively cooler waters are upwelled from the Equatorial Undercurrent that shoals as it flows from west to east (Kessler, 2006; Sloyan et al., 2003). Note that the cold tongue never looks like the mean of Fig. 3a, nor is all variability accounted for by the seasonal and ENSO (El Niño–Southern Oscillation, see Appendix) patterns of Figs. 3b and c; tropical instability waves markedly distort the fronts along the northern and southern edges so that the “tongue” looks more like an “auger” (Willett et al., 2006). The cold tongue seasonal amplitude is $\pm 1\text{--}3\text{ }^{\circ}\text{C}$, with coldest temperatures in September–October. Eastern boundary current waters are marked by thermal fronts where they reach the eastern Pacific warm pool off Ecuador and the southern end of Baja California. These waters have high seasonal amplitudes of surface temperature ($\pm > 3\text{ }^{\circ}\text{C}$). The semiannual harmonic makes only a small contribution to the seasonal cycle of surface temperature – the semiannual amplitude is 0.1–0.3 times the annual amplitude – except near the thermal equator (not shown). Surface temperature variability associated with ENSO is highest ($\pm 1\text{--}2\text{ }^{\circ}\text{C}$) along the equator and in eastern boundary current waters, and lowest in the warm pool. High-frequency variability associated with equatorial and coastal Kelvin waves during El Niño events is not resolved by the ENSO component of our analysis.

Smaller-scale patterns of mean surface temperature are also related to important oceanographic processes. The local minimum at 9°N, 89°W marks the Costa Rica Dome, an oceanic upwelling center where the thermocline ascends to very near the sea surface (see Fig. 9). The dome is associated with the terminus of the equatorial current system (Wyrtki, 1964a; Fiedler, 2002; Kessler, 2006) and is influenced by mesoscale coastal eddies (Willett et al., 2006). Surface temperature minima extending off the coast from the Gulfs of Tehuantepec, Papagayo, and Panama are associated with seasonal wind jets (Willett et al., 2006). The temperature minimum on the west side of the Galapagos is due to upwelling of Equatorial Undercurrent water (Kessler, 2006).

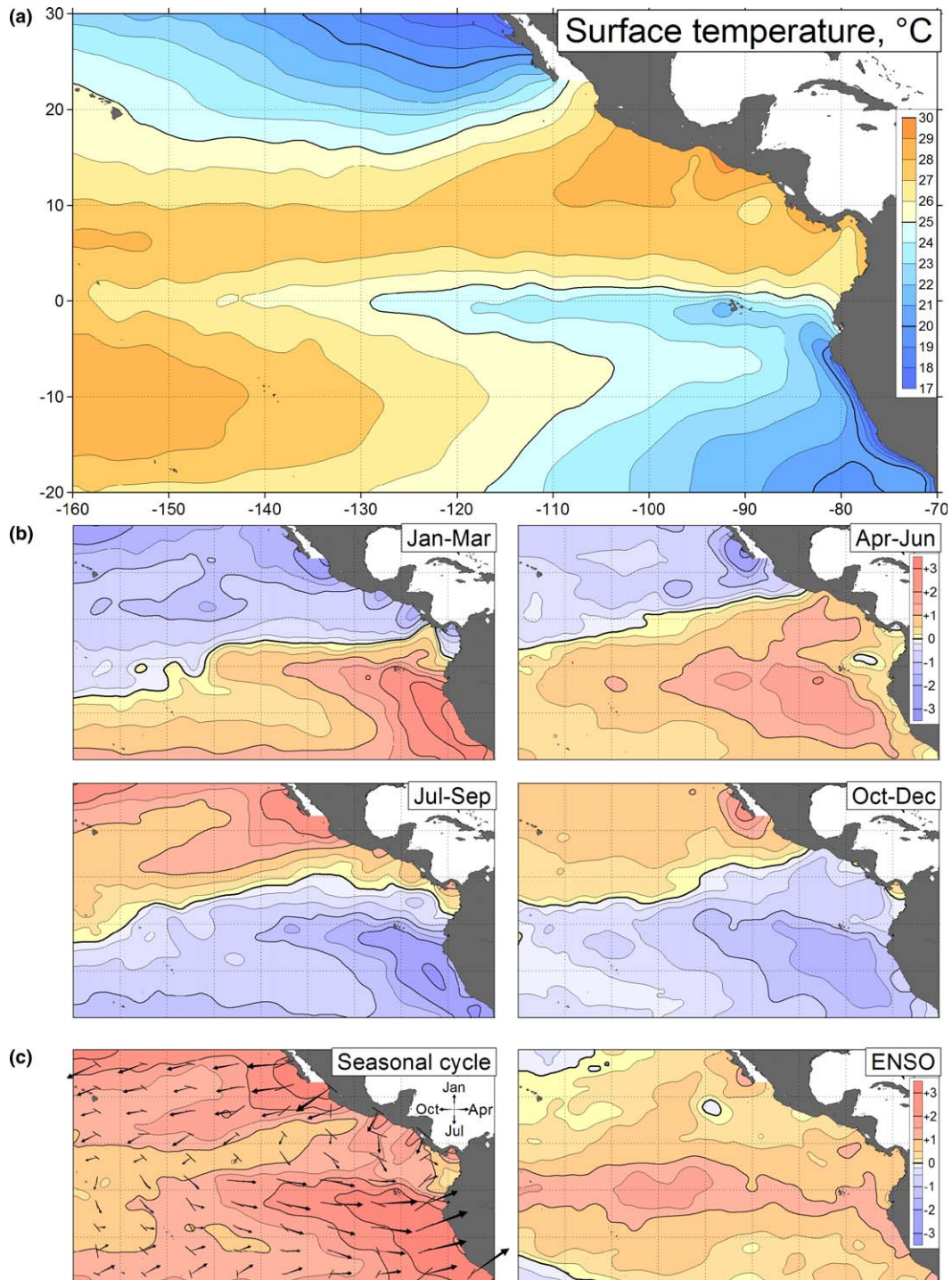


Fig. 3. Surface temperature, from WOD01 BT, CTD and bottle data: (a) mean; (b) quarterly deviations from the mean; (c) seasonal cycle and ENSO effect (see Appendix). Seasonal cycle magnitude is the sum of annual and semiannual amplitudes; annual phase (timing of maximum) is indicated by arrows and semiannual phase by fine lines (length scaled to log of amplitude).

Eastern tropical Pacific mean surface salinity (Fig. 4) is lowest in the Gulf of Panama (29–31), where extreme local rainfall systems enhance the summer monsoon rainfall along the Pacific slope of Central America (Amador et al., 2006). Westward transport of water vapor across the Isthmus of Panama also contributes

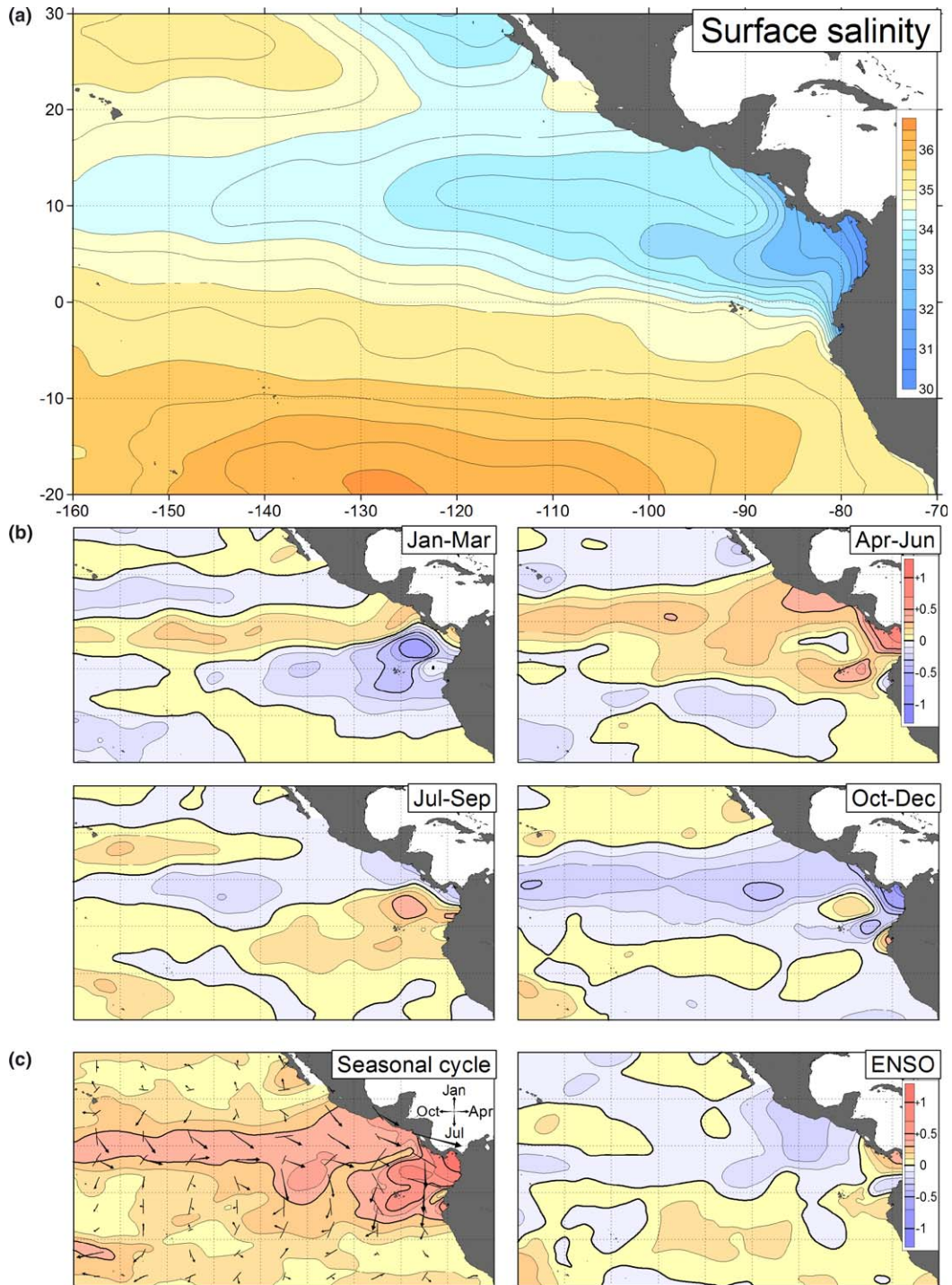


Fig. 4. Surface salinity, from WOD01 bottle, surface and CTD data: (a) mean; (b) quarterly deviations from the mean; (c) seasonal cycle and ENSO effect (see Appendix). Seasonal cycle magnitude is the sum of annual and semiannual amplitudes; annual phase (timing of maximum) is indicated by arrows and semiannual phase by fine lines (length scaled to log of amplitude).

to the high net precipitation at this location (Benway and Mix, 2004). Another mass of low-salinity water is found off Baja California, a signature of California Current Water. Salinity of surface waters increases towards the subtropical gyres to the south and northwest of the eastern tropical Pacific. Low-salinity surface

waters (<34.5) are found in a zonal band centered along $10\text{--}11^\circ\text{N}$ west of 110°W and $5\text{--}7^\circ\text{N}$ east of 100°W . This low-salinity water does not coincide with the warm-water band described above. Rather, it lies beneath the mean position of the Intertropical Convergence Zone (ITCZ) where precipitation exceeds evaporation (Fig. 5).

Seasonal variability of quarterly deviations on the north and south of the low-salinity band beneath the ITCZ, notably the reversal of phase between January–March and July–September (Fig. 4b), and the minimum in seasonal variability along $\sim 7^\circ\text{N}$ latitude (Fig. 4c), reflects the annual march with the sun of the ITCZ and associated rainfall (Amador et al., 2006). Seasonal variability is relatively high ($>\pm 0.3$) here, but much higher near the Gulf of Panama. Where seasonal variability is low, the semiannual harmonic makes a significant contribution to the seasonal cycle (semiannual/annual amplitude > 0.5). This might indicate that the annual harmonic does not adequately describe the seasonal cycle where variability is low and the data are relatively noisy.

The pattern of ENSO variability of surface salinity in near-equatorial waters is roughly similar to the interannual EOF of Delcroix (1998) and reflects the El Niño precipitation increase that is centered along 5°N east of the dateline (Xie and Arkin, 1997). Variability of surface salinity associated with ENSO exceeds ± 0.2 in a few locations along the coast of Central America. Explanation of the ENSO-related surface salinity anomalies here must include differential effects on oceanic and terrestrial rainfall in this region: oceanic rainfall increases between the equator and 10°N near the coast of Central America, but decreases over land (Dai and Wigley, 2000; Hastenrath, 2002), especially over the normally wet El Choco rainforest in western Colombia, thus reducing runoff and increasing salinity in the Gulf of Panama. Advective effects must also be important.

A global perspective for the patterns of eastern tropical Pacific surface temperature and salinity described above is illustrated in Fig. 6. The eastern Pacific warm pool is warmer than any surface water in the tropical Atlantic, but not as warm as the much larger western Pacific warm pool in the western Pacific and eastern Indian Oceans. The equatorial cold tongue in the eastern Pacific is colder than the eastern Atlantic equatorial cold tongue; there is no such feature in the Indian Ocean. Surface salinity values as low as in the eastern tropical Pacific (<33) are not found in any other region between the North Pacific Subarctic Front and the Antarctic Convergence, except in coastal waters with large riverine input (e.g. the Columbia River off the western

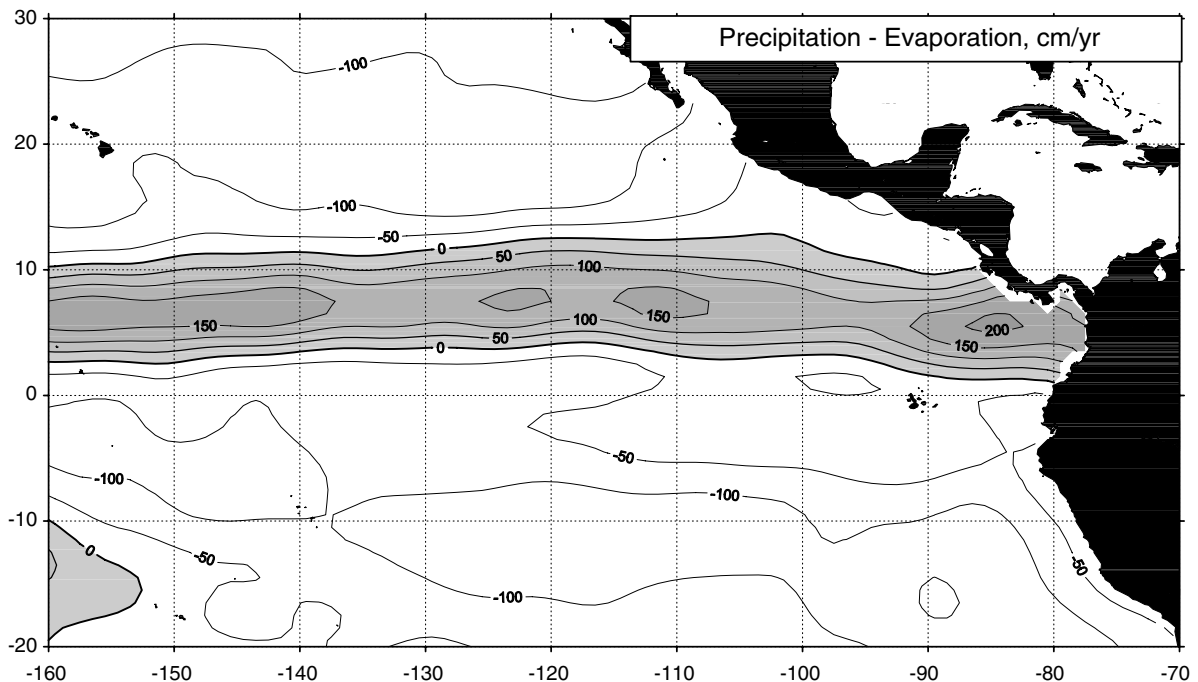


Fig. 5. Mean eastern tropical Pacific precipitation minus evaporation rate. From da Silva et al. (1994). Net precipitation is shaded.

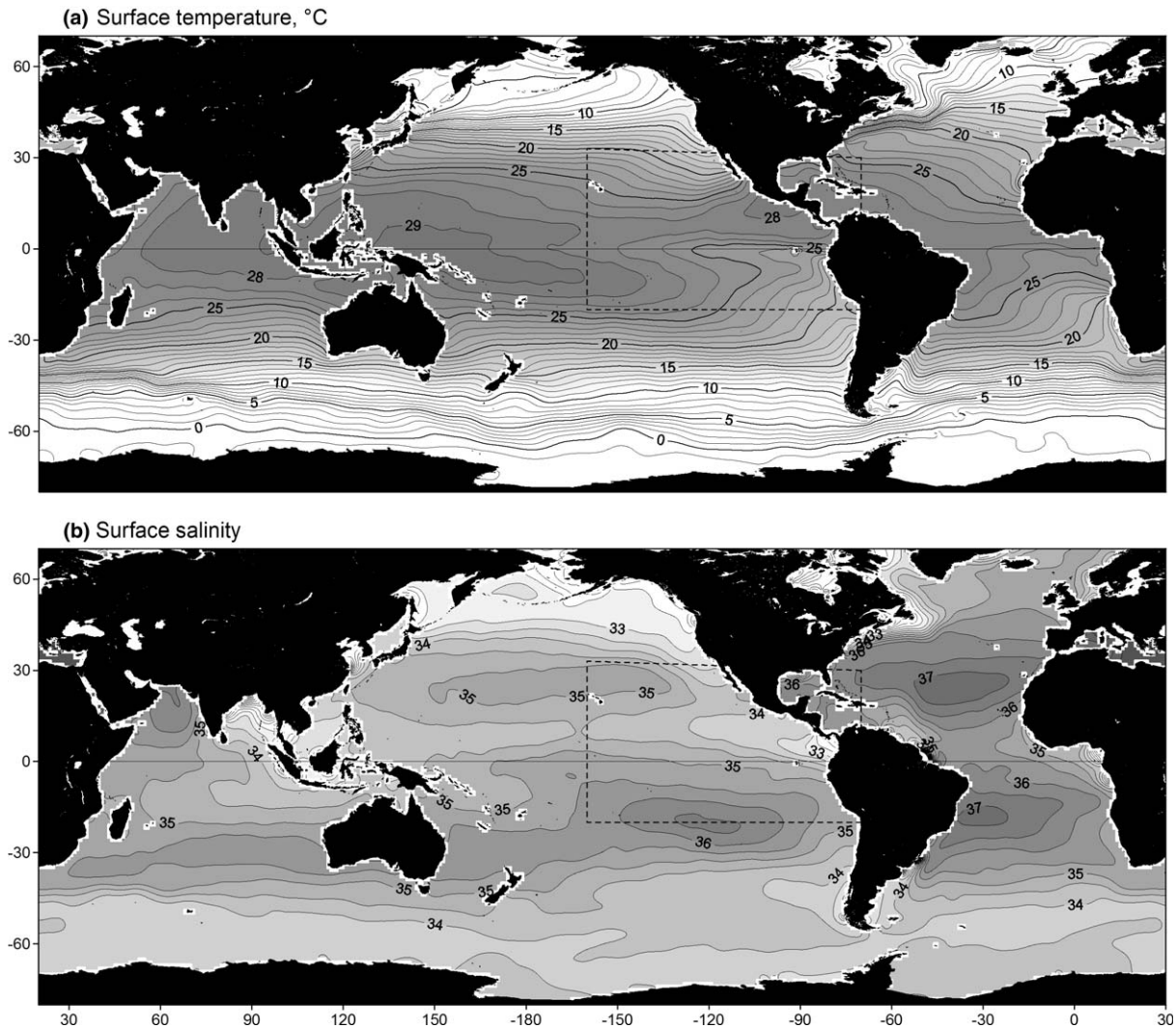


Fig. 6. Global surface temperature and salinity from World Ocean Atlas 2001 (see Appendix): (a) mean surface temperature; (b) mean surface salinity. Dashed rectangles mark extent of Figs. 3 and 4.

United States). This reflects both the excess of precipitation over evaporation beneath the ITCZ (Fig. 5) and riverine input to the Gulf of Panama off the western slope of the Andes in Colombia.

The eastern tropical Pacific surface water masses defined by the patterns of surface temperature and salinity in Figs. 3 and 4 are Tropical Surface Water (TSW: $T > 25^\circ$, $S < 34$) north of the equator and Equatorial Surface Water (ESW: $T < 25^\circ$, $S > 34$) along the equator (Wyrtki, 1966). These water masses are separated by the equatorial front located nearly on the equator to the east of the Galapagos and 2–3° north of the equator to the west. Subtropical Surface Water masses (STSW: $S > 35$) are located in the North and South Pacific central gyres (Fig. 6), to the northwest and southwest of the eastern tropical Pacific, where evaporation exceeds precipitation. Although Subtropical Surface Waters are sometimes labeled Tropical Surface Waters (Tsuchiya, 1968; Tsuchiya and Talley, 1998), it is important to differentiate the fresher TSW in the eastern tropical Pacific from the saltier STSW in the subtropics. The distinct characteristics of these water masses are determined mainly by local surface fluxes of heat and freshwater (Wyrtki, 1966; Large and Nurser, 2001). Wyrtki (1967) recognized that although Equatorial Surface Water lies between TSW and the STSW of the South Pacific, it is not a simple mixing product of those two water masses. Salinity of ESW is intermediate, but for most of the year, ESW is considerably colder than TSW and STSW. This is the result of both equatorial upwelling

and advection of Peru Current water. The cold, low-salinity surface water off Baja California is California Current Water, originating in the subarctic North Pacific (Sverdrup et al., 1942).

3. Upper ocean density structure

Tropical pycnoclines are relatively strong (high $d\sigma/dz$) and shallow in the global context (Fig. 7); the pycnocline in the eastern tropical Pacific is an extreme case. It is primarily a thermocline, in that most of the density stratification is due to a vertical temperature gradient, but is reinforced by a halocline. The structure of the near-surface water column in the eastern tropical Pacific, and to a lesser extent in the eastern tropical Atlantic, is unusual because the stratification characteristic of tropical oceans is extreme in this region: the thermocline is shallow and strong (temperature gradient $|dT/dz|$ is high), and there is a coincident strong halocline beneath the warm, low-salinity TSW (Fig. 8). In Wyrтки's (1964b) study of thermal structure, the region is characterized by a permanent shallow thermocline, with a temperature gradient that usually exceeds $1\text{ }^\circ\text{C}$ per 10 m and a large temperature difference between the top and bottom of the thermocline. Deepening of the pycnocline towards the subtropical gyres reflects the geostrophic balance of the large-scale basin circulation.

Mean thermocline depth (depth of maximum $|dT/dz|$, see Appendix) generally deepens from east to west (Fig. 9a). Two zonal thermocline ridges are consistent with the surface circulation that is predominantly zonal west of 110°W (Kessler, 2006). The equatorial thermocline ridge lies along the equator, coincident with the equatorial cold tongue. The countercurrent thermocline ridge along 10°N is named for the North Equatorial Countercurrent that flows at the surface over its southern flank. These zonal thermocline ridges correspond to sea surface troughs named by Wyrтки (1975a). The countercurrent thermocline ridge is marked by local peaks or depth minima at 89°W (the Costa Rica Dome) and 126°W . The saddle in the countercurrent thermocline ridge at 109°W and the "Tehuantepec bowl" in the thermocline centered at 13°N , 105°W affect geostrophic circulation and are discussed by Kessler (2006). The thermocline is strongest between 5°S and 15°N , except directly on the equator (Fig. 10). The vertical spreading of isotherms in the equatorial thermocline (see Fig. 15) is associated both with the geostrophy of the Equatorial Undercurrent and with equatorial divergence and upwelling (Kessler, 2006).

The seasonal cycle of thermocline depth (Fig. 9c) is of smallest amplitude ($<\pm 10\text{ m}$) in the far eastern tropical Pacific, between the Galapagos and Costa Rica and along the SW Mexican coast, and along the axis of the countercurrent thermocline ridge. Opposite phasing of the seasonal cycle to the north and south of the ridge (Fig. 9c, April–June and October–December in Fig. 9b) corresponds approximately to the thermal equator pattern seen in the surface temperature seasonal cycle (Fig. 3). This shows that seasonality of net heat flux and wind mixing influences both surface temperature and thermocline depth. Seasonal variability increases to the north and south, except for a slight decrease at the equator, to $>\pm 50\text{ m}$ in the subtropical gyres. This pattern reflects the development of a seasonal thermocline above the permanent thermocline in the subtropics and at higher latitudes (Wyrтки, 1964b), although the present analysis defines only one thermocline because the permanent thermocline dominates thermal structure in the eastern tropical Pacific. At all latitudes, seasonal variability of thermocline depth is lowest toward the coast where the mean depth is shallowest. As for surface temperature and salinity, the semiannual harmonic makes only a small contribution to the seasonal cycle of thermocline depth (semiannual/annual amplitude is 0.2–0.4), except where seasonal variability is low, in this case along the countercurrent ridge and near the Central American coast. The ENSO pattern shows that the thermocline deepens by 5–10 m in much of the eastern tropical Pacific during El Niño events, especially along the equator, but shoals towards the west along the equator and in the subtropics (Wyrтки, 1975b). ENSO-related tilting of the Pacific equatorial thermocline is reviewed by Wang and Fiedler (2006).

Mixed layer depth (isothermal layer depth, see Appendix) shows spatial and temporal patterns (Fig. 11) that are very similar to those of thermocline depth (Fig. 9). Above the equatorial and countercurrent thermocline ridges, and in eastern boundary current waters, the mixed layer is 10–20 m shallower than the thermocline. Above the thermocline trough between these ridges, the mixed layer is 30–50 m shallower than the thermocline. Poleward and westward of the thermocline ridges, in the subtropical gyres, the mixed layer is 70–100 m deep, but the thermocline is up to 100 m deeper. Differences in patterns of temporal variability of mixed layer and thermocline depths are apparent. For example, the annual cycles of both variables have

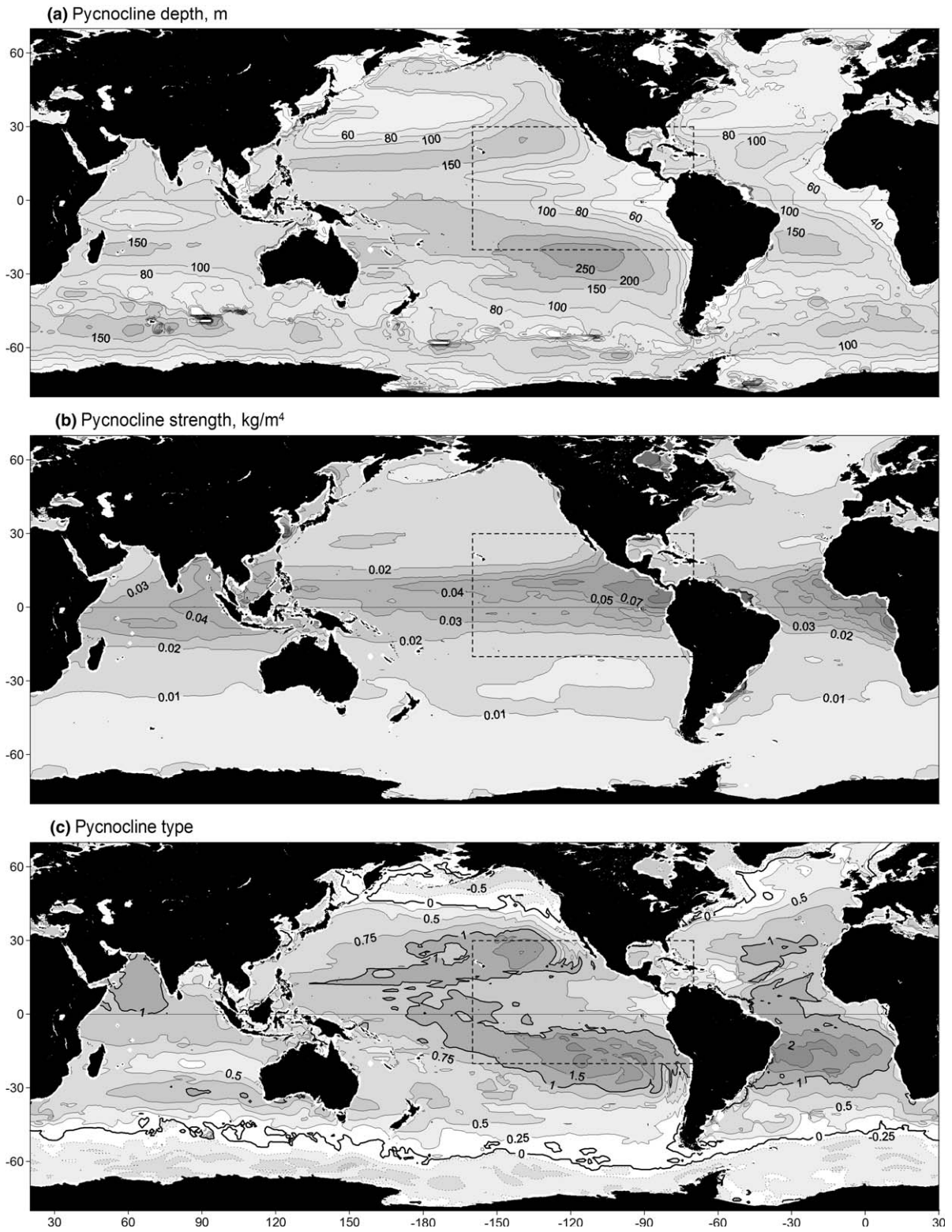


Fig. 7. Global pycnocline parameters derived from World Ocean Atlas 2001 gridded fields at standard depths (see Appendix): (a) depth; (b) strength; (c) type: halocline (<0), thermocline (>0), thermocline opposed by a destratifying halocline (>1). Dashed rectangles mark extent of Figs. 9 and 10.

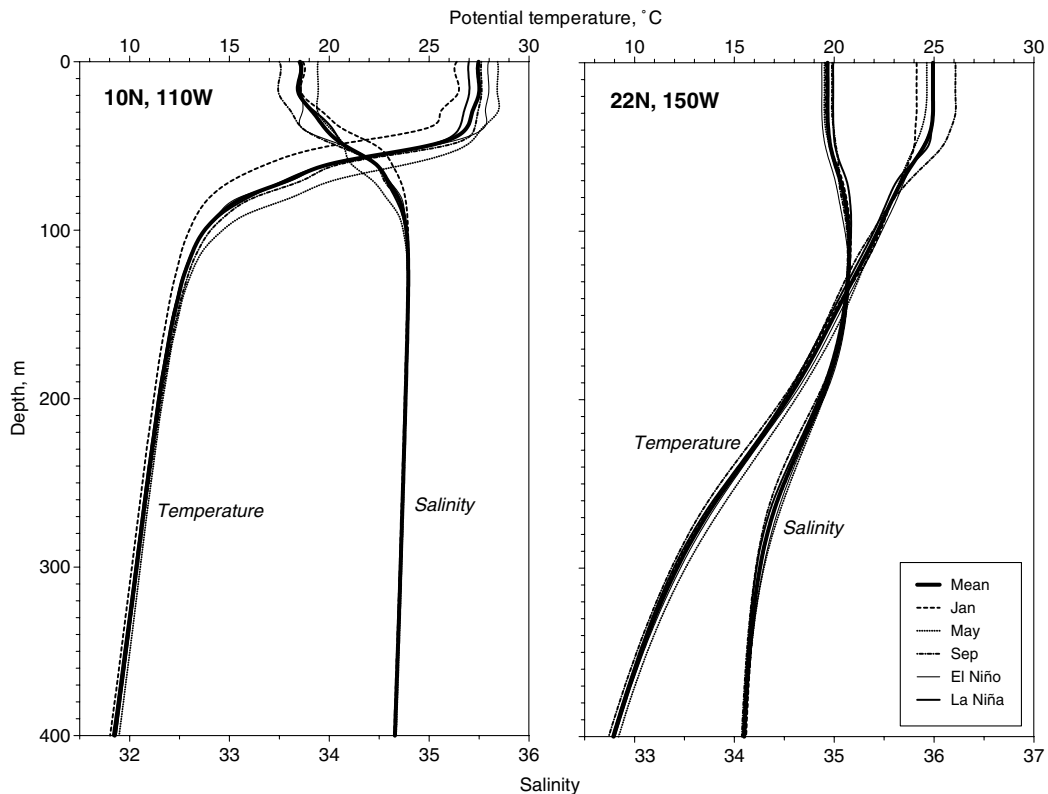


Fig. 8. Mean temperature and salinity profiles, from WOD01 CTD data, at two locations: (left) 10°N, 110°W, typical of the eastern tropical Pacific; (right) 22°N, 150°W, typical of the northern subtropical Pacific.

a minimum or node at 8–10°N, but to the north and south of this node, changes in mixed layer depth lead changes in thermocline depth by 2–3 months (Figs. 9c and 11c). This phase difference is also manifested as differences between the two variables in patterns of quarterly deviations (Figs. 9b and 11b). The semiannual harmonic contributes much more to the seasonal cycle of mixed layer depth than it does for thermocline depth. ENSO variability is more focused on the equator for mixed layer depth than for thermocline depth, perhaps reflecting a greater influence of local wind forcing on mixed layer depth and remote forcing on thermocline depth.

A “barrier layer” beneath the well-mixed surface layer, the result of a strong halocline overlying a deeper thermocline, has been shown to be important in regions of the global tropical ocean where rainfall freshens a surface layer that is mixed to a depth significantly less than the thermocline depth (Lukas and Lindstrom, 1991). In the western tropical Pacific, mean barrier layer thicknesses exceed 30 m (Fig. 12) and seasonal values can exceed 50 m (Sprintall and Tomczak, 1992). In contrast, barrier layer thickness is <10 m in most of the eastern tropical Pacific, where the shallow thermocline precludes development of a thick barrier layer even where rainfall is high. Ando and McPhaden (1997) showed a similar pattern across the tropical Pacific, based on analysis of individual CTD profiles and local vertical gradient definitions of isothermal and mixed layer depths. However, Cronin and Kessler (2002) found evidence of development of a significant barrier layer on the equator at 110°W, for brief periods following rainstorms during the 1997–1998 El Niño, when winds were weak and rainfall was enhanced.

4. Surface nutrients and oxygen

Nutrient concentrations in eastern tropical Pacific surface waters are generally high in equatorial and eastern boundary current surface waters (Fig. 13). The elevated nutrients and reduced oxygen saturation levels

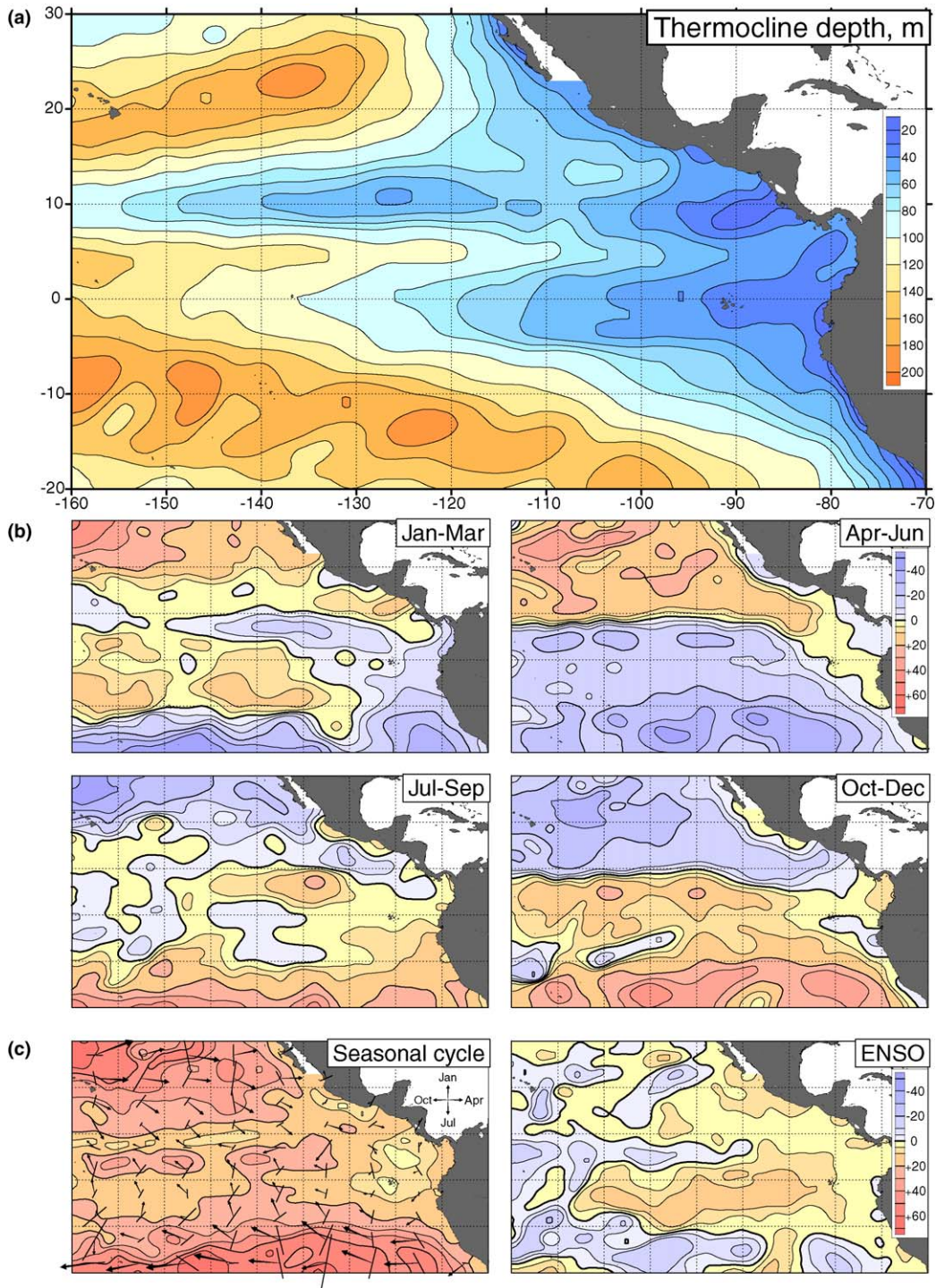


Fig. 9. Thermocline depth, from WOD01 BT and CTD data: (a) mean; (b) quarterly deviations from the mean; (c) seasonal cycle and ENSO effect (see Appendix). Seasonal cycle magnitude is the sum of annual and semiannual amplitudes; annual phase (timing of maximum) is indicated by arrows and semiannual phase by fine lines (length scaled to log of amplitude).

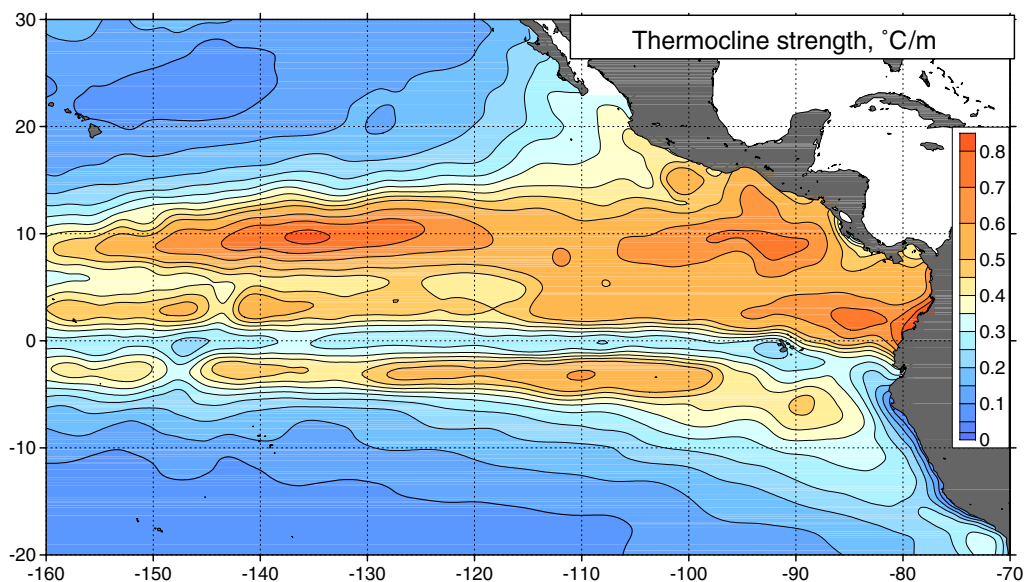


Fig. 10. Mean thermocline strength, $^{\circ}\text{C m}^{-1}$, from WOD01 BT and CTD data (see Appendix).

(Fig. 13d) of these surface waters reflect the input of pycnocline waters by equatorial and coastal upwelling. Nutrient concentrations are lower in Tropical Surface Water, although phosphate and nitrate are elevated in the region of the Costa Rica Dome by wind mixing of water from the shallow nutricline (Wooster and Cromwell, 1958). Surface nutrient concentrations are lowest in the subtropical gyres to the northwest and southwest of the eastern tropical Pacific. Available nutrient and oxygen data are insufficient to resolve seasonal and ENSO variability. Pennington et al. (2006) discuss the significance of the relatively high nutrient but low chlorophyll levels (HNLC) in the eastern equatorial Pacific.

5. Thermocline and intermediate waters

Beneath the warm, low-salinity Tropical Surface Water in the eastern Pacific warm pool north of the equator, a very strong thermocline/halocline separates surface and subpycnocline waters, but does not contain a distinct water mass of any substantial volume. This cooler, more saline thermocline water is upwelled at the equator and contributes to the formation of Equatorial Surface Water (Wyrтки, 1967; Tsuchiya and Talley, 1998). Locally cool temperature, increased salinity, and high nutrients (Fig. 13) at the surface are a signature of upwelling that can also be seen along the coast of Peru and at the Costa Rica Dome (Wyrтки, 1964a).

South of the equator, South Pacific Subtropical Surface Water (Wyrтки, 1966, 1967) is subducted northward into the thermocline and forms a salinity maximum in the upper thermocline north of 10°S (Figs. 14a, 15a and 16a). West of the Galapagos, this water is also marked by phosphate, silicate, and nitrate minima (Figs. 15b and 16b). This Subtropical Underwater (STUW; O'Connor et al., 2002), formerly called Subtropical Subsurface Water (Wyrтки, 1966) is found along the equator at ~ 100 m (see Fig. 18a). The South Pacific STUW subduction region is between 150°W and 90°W , and south of 20°S (O'Connor et al., 2002). North Pacific Subtropical Surface Water is subducted southward into the thermocline north of 20°N and forms a subsurface salinity maximum that meets the Subtropical Underwater from the South Pacific at about 10°N (Fig. 16a). As there is no North Pacific source east of the Galapagos, STUW extends north of the equator from the south as a broad salinity maximum along 88°W (Fig. 14a). Johnson and McPhaden (1999) discuss the importance of this water mass as a pathway for the propagation of thermal anomalies from the South Pacific to the equatorial pycnocline. It is noted that zonal velocities are one to two orders of magnitude greater than meridional velocities even below the surface layer (Kessler, 2006).

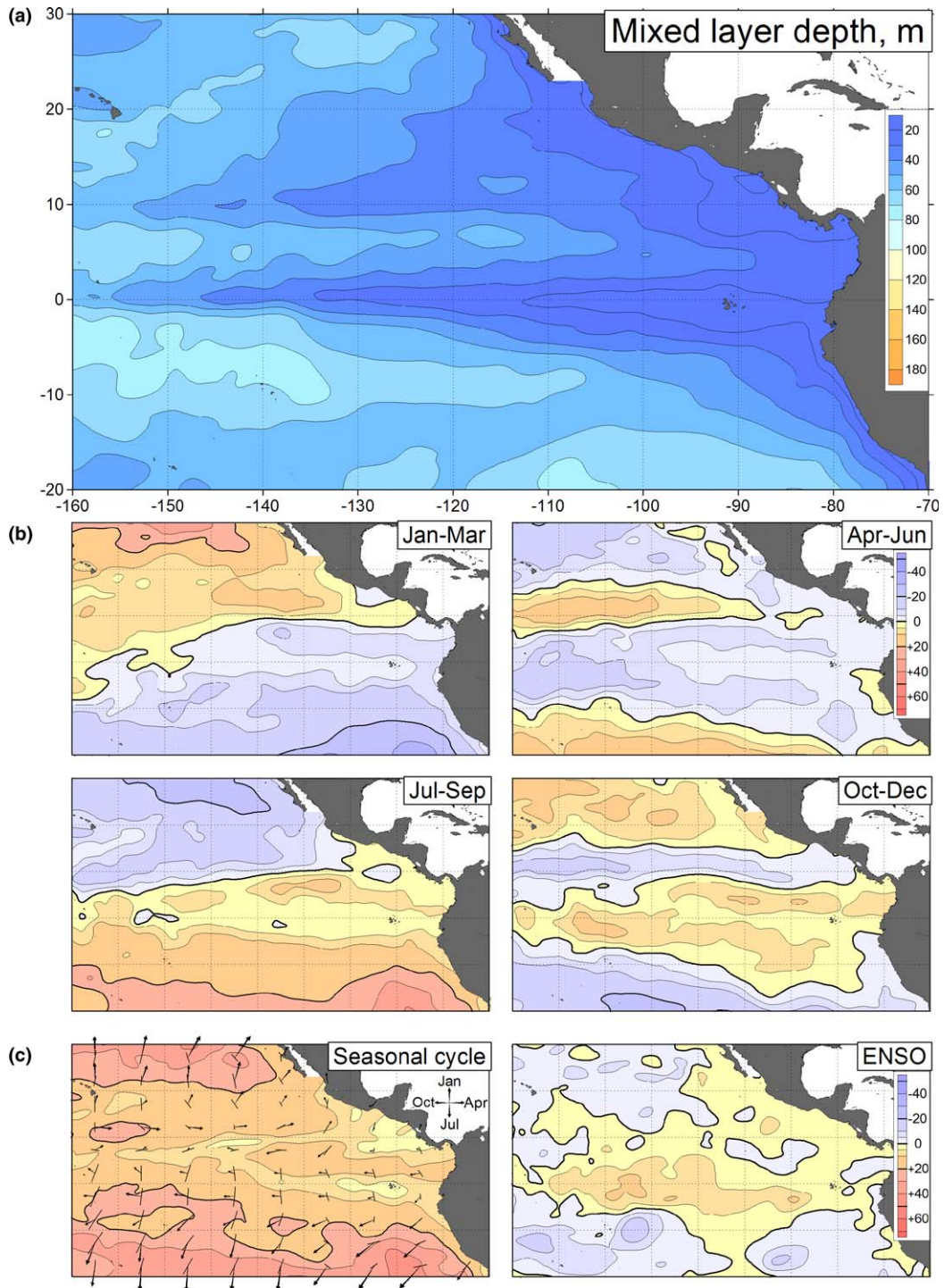


Fig. 11. Mixed layer depth, from WOD01 BT and CTD data: (a) mean, (b) quarterly deviations from the mean, (c) seasonal cycle and ENSO effect (see Appendix). Seasonal cycle magnitude is the sum of annual and semiannual amplitudes; annual phase (timing of maximum) is indicated by arrows and semiannual phase by fine lines (length scaled to log of amplitude).

The equatorial thermocline just beneath the STUW, at temperatures of 13–22 °C, is ventilated in the eastern South and North Pacific, as relatively thick surface layers called South and North Pacific Eastern Subtropical Mode Water (SPESTMW and NPESTMW; Hanawa and Talley, 2001). “Mode Water” is a name given to a

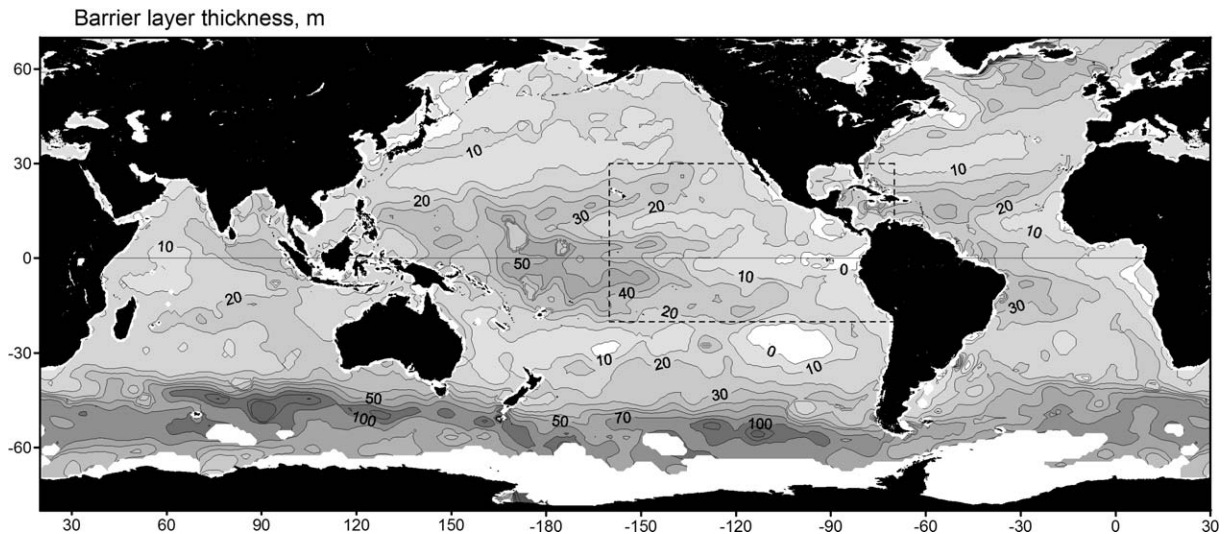


Fig. 12. Global barrier layer thickness (m, difference between isothermal layer depth and mixed layer depth) from World Ocean Atlas 2001 (see Appendix). Barrier layer thickness is undefined in blank areas of the Southern Ocean, where the water column is essentially isothermal to the bottom. Dashed rectangle marks extent of Fig. 11.

layer of vertically near-homogeneous water formed by surface mixing, usually subducted to within or near the top of the permanent pycnocline and, therefore, apparent as a pycnostad (pycnostads or thermostads are layers of relatively low vertical density or temperature gradient). There are no major water property signatures of these mode waters in the equatorial thermocline; they lie between the STUW and the 13 °C thermostad described below. Both the North and South Pacific Eastern Subtropical Mode Waters involve subduction of waters where thermocline stratification is opposed by a destratifying halocline (Fig. 7c).

SPESTMW is found in the southeastern subtropical South Pacific, near the southern subtropical boundary of the eastern tropical Pacific (Tsuchiya and Talley, 1998; Hanawa and Talley, 2001; Wong and Johnson, 2003). Its temperature and salinity ranges are 13–20 °C and 34.3–35.5. NPESTMW is formed by deep winter mixing in the northern subtropical gyre northeast of Hawaii and is visible in individual sections (Hautala and Roemmich, 1998) as a thermostad/pycnostad and potential vorticity or stratification minimum in the 16–22 °C range at ~100 m; however, it is not apparent in the mean 150°W section (Fig. 16). Because the South Pacific subtropical circulation connects directly to the equatorial circulation, whereas the North Pacific's is separated by the North Equatorial Countercurrent, the SPESTMW may have a greater impact on the equatorial thermocline than does NPESTMW. On the other hand, tritium and anthropogenic ³He sections from WOCE (World Ocean Circulation Experiment) show a sharp demarcation at the equator between thermocline waters ventilated in the South Pacific and North Pacific (Jenkins, 1996), suggesting that both subtropical gyres contribute to the equatorial thermocline.

Thermostads on either side of the equator, below the primary shallow thermocline/pycnocline and associated with narrow eastward jets, are clear features of the equatorial structure in the central and eastern Pacific. Montgomery and Stroup (1962) originally described a water mass, 13 °C Equatorial Water, corresponding to these features and visible as a thermostad/pycnostad between 5°S and 5°N (12–14 °C at 110°W in Fig. 15, 11–13 °C at 150°W in Fig. 16). We will use the name 13 °C Water. The secondary permanent thermocline below this thermostad, along with a halocline in some cases, is more apparent in individual than in mean sections (135°W: Tsuchiya and Talley, 1996; 110°W: Hayes et al., 1983). The 13 °C Water (13CW) is bounded to the north and south by steeply sloping isopycnals associated with eastward Subsurface Countercurrents, also known as Tsuchiya jets (see Kessler, 2006). The thermostad that defines 13CW is clearly seen in a mean equatorial section (Fig. 18).

Tsuchiya (1981) hypothesized, based on isopycnal property mapping, that the source of water in the 13 °C thermostad is surface water in the western South Pacific. This picture has recently been modified to account

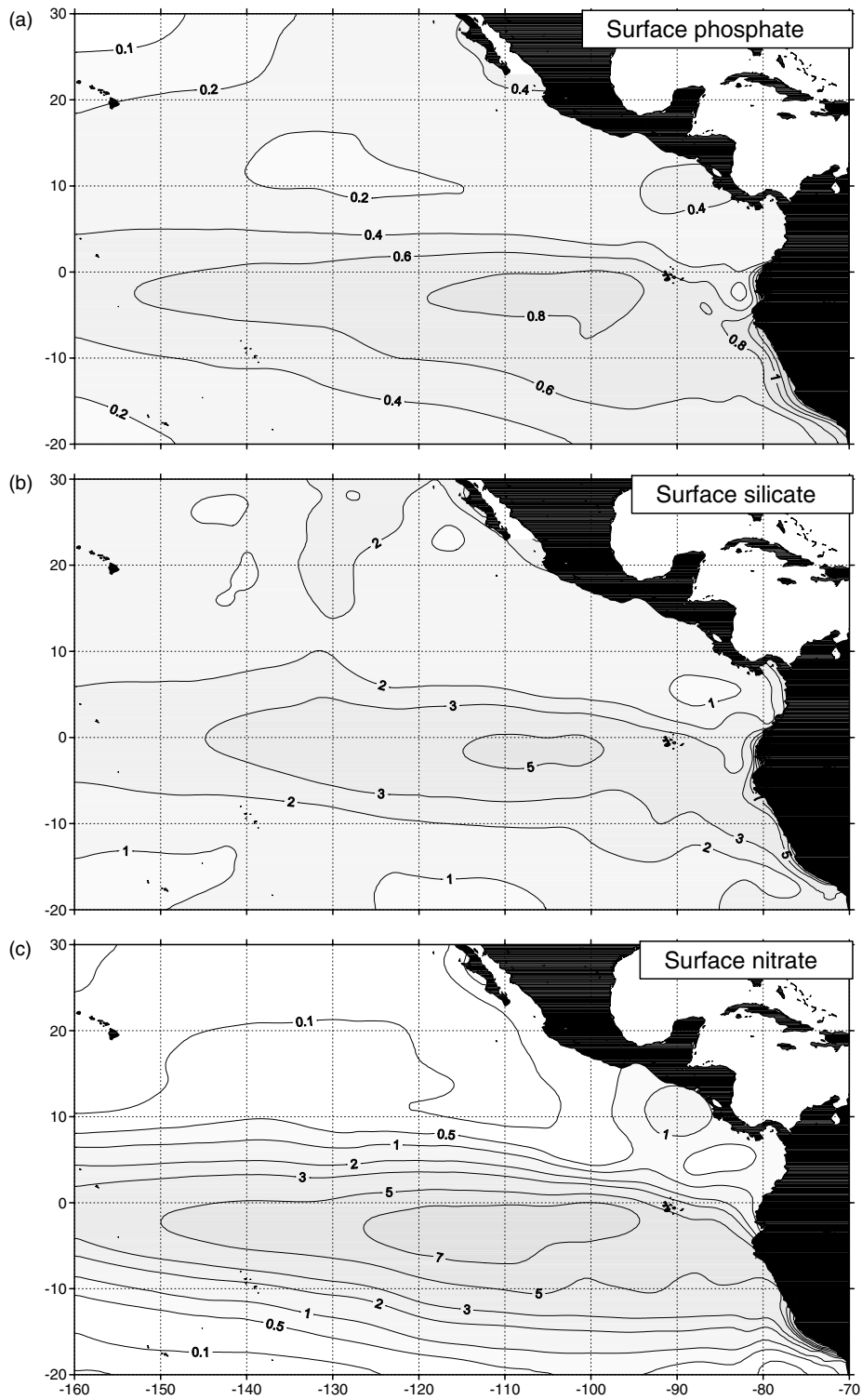


Fig. 13. Mean surface nutrient concentrations, $\mu\text{mol kg}^{-1}$, from WOD01 bottle data (see Appendix): (a) phosphate (PO_4); (b) silicate (Si(OH)_4); (c) nitrate (NO_3).

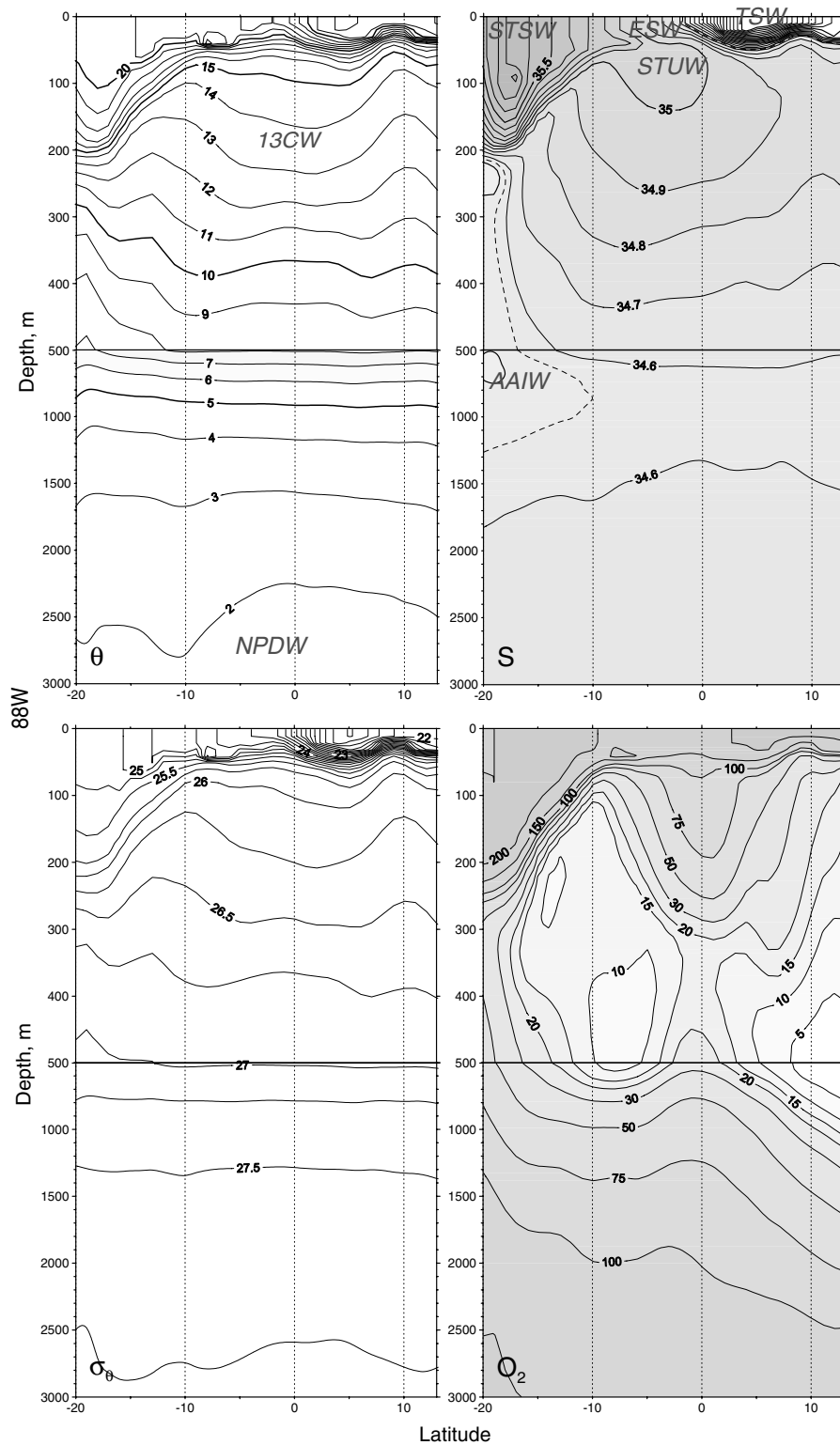


Fig. 14a. Mean meridional sections along 88°W from WOD01 CTD and bottle data (see Appendix): potential temperature (θ , °C, referenced to 0 db), salinity (S), potential density (σ_θ , kg m^{-3}), and dissolved oxygen concentration (O_2 , $\mu\text{mol kg}^{-1}$). Water masses: Tropical Surface Water (TSW), Equatorial Surface Water (ESW), Subtropical Surface Water (STSW), Subtropical Underwater (STUW), 13 °C Water (13CW), Antarctic Intermediate Water (AAIW), North Pacific Deep Water (NPDW).

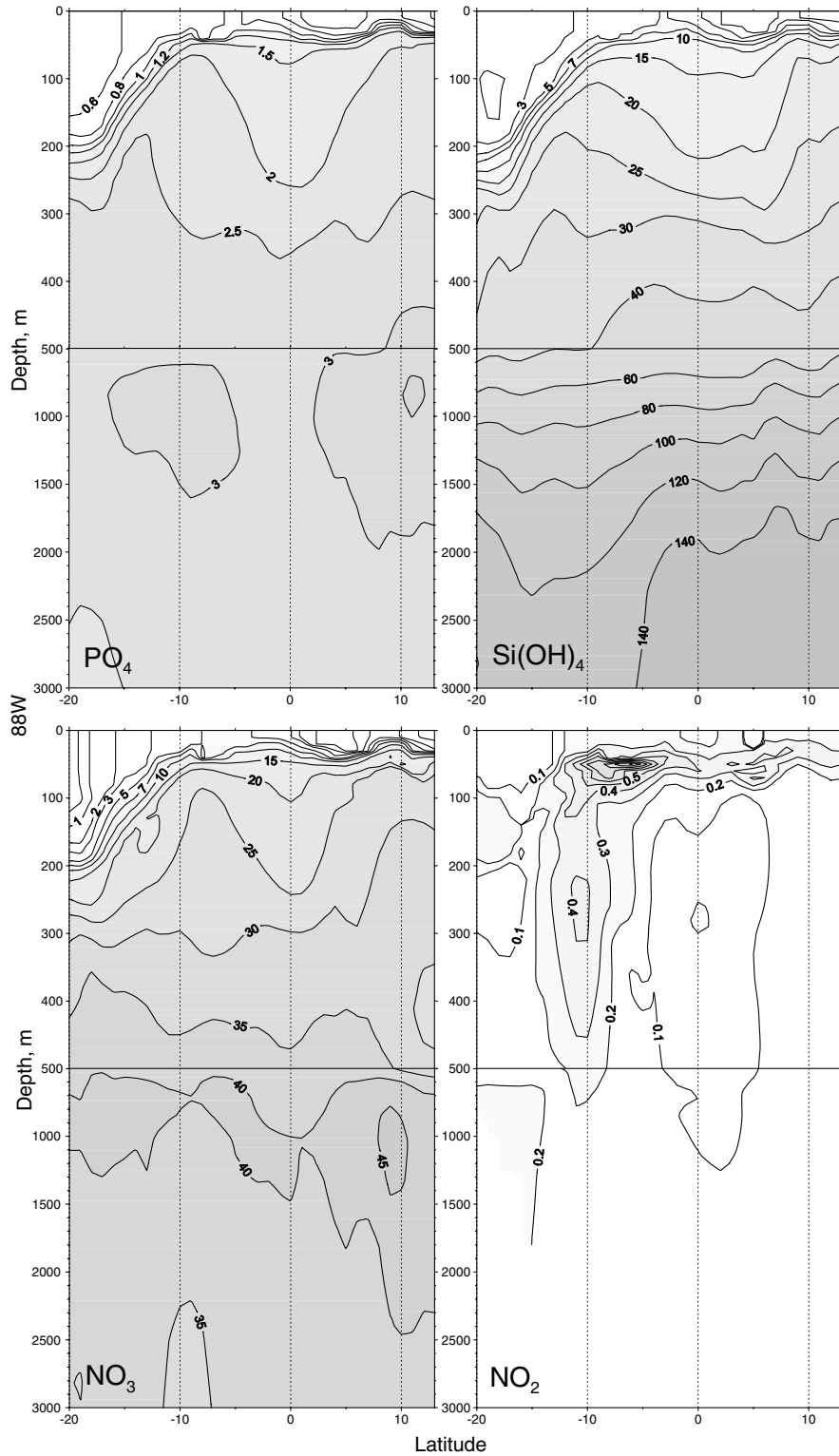


Fig. 14b. Mean meridional sections of nutrients ($\mu\text{mol kg}^{-1}$) along 88°W from WOD01 bottle data (see Appendix): phosphate (PO_4), silicate (Si(OH)_4), nitrate (NO_3), and nitrite (NO_2).

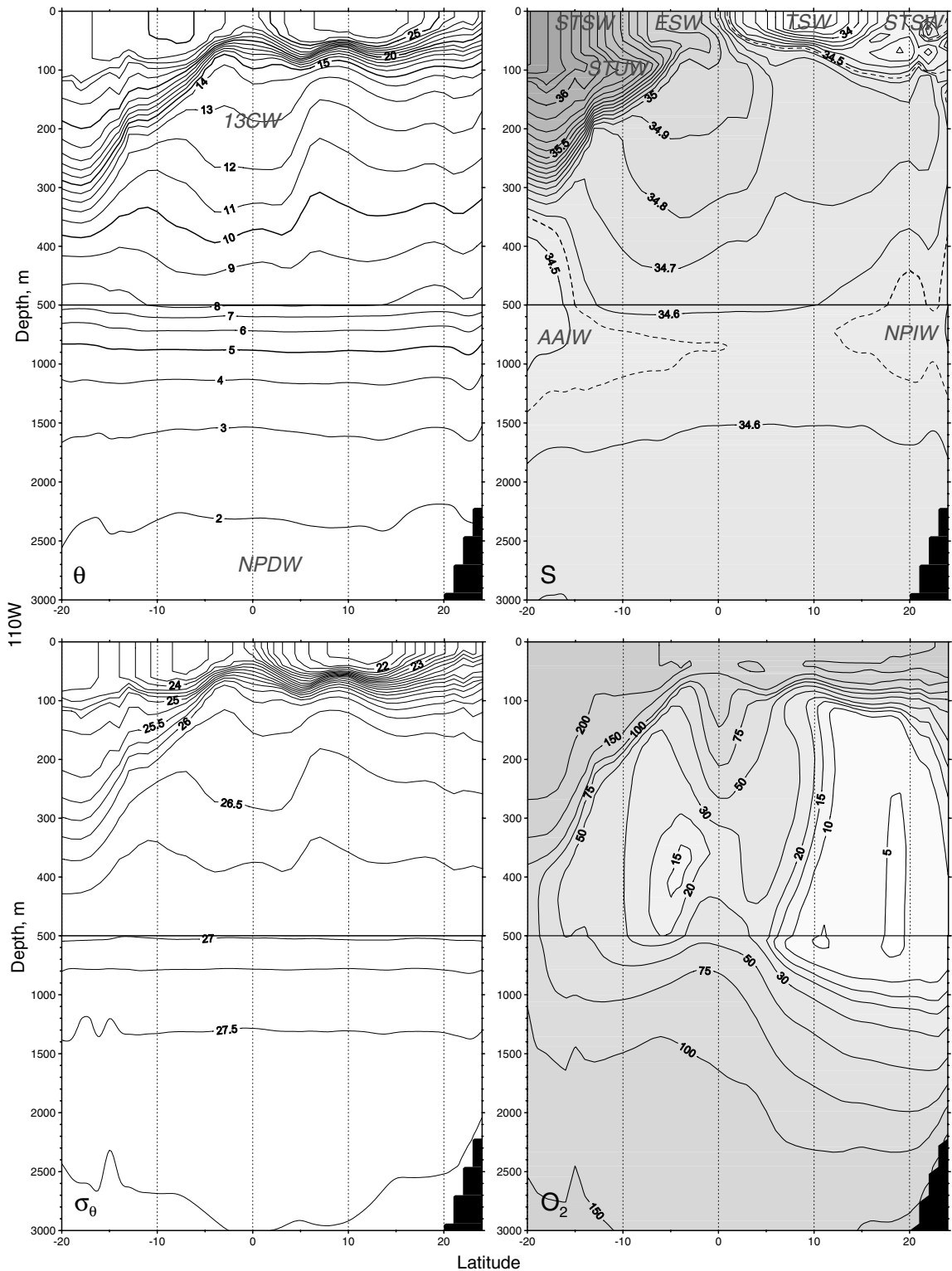


Fig. 15a. Mean meridional sections along 110°W from WOD01 CTD and bottle data (see Appendix): potential temperature (θ , °C, referenced to 0 db), salinity (S), potential density (σ_θ , kg m^{-3}), and dissolved oxygen concentration (O_2 , $\mu\text{mol kg}^{-1}$). Water masses: Tropical Surface Water (TSW), Equatorial Surface Water (ESW), Subtropical Surface Water (STSW), Subtropical Underwater (STUW), 13 °C Water (13CW), Antarctic Intermediate Water (AAIW), North Pacific Intermediate Water (NPIW), North Pacific Deep Water (NPDW).

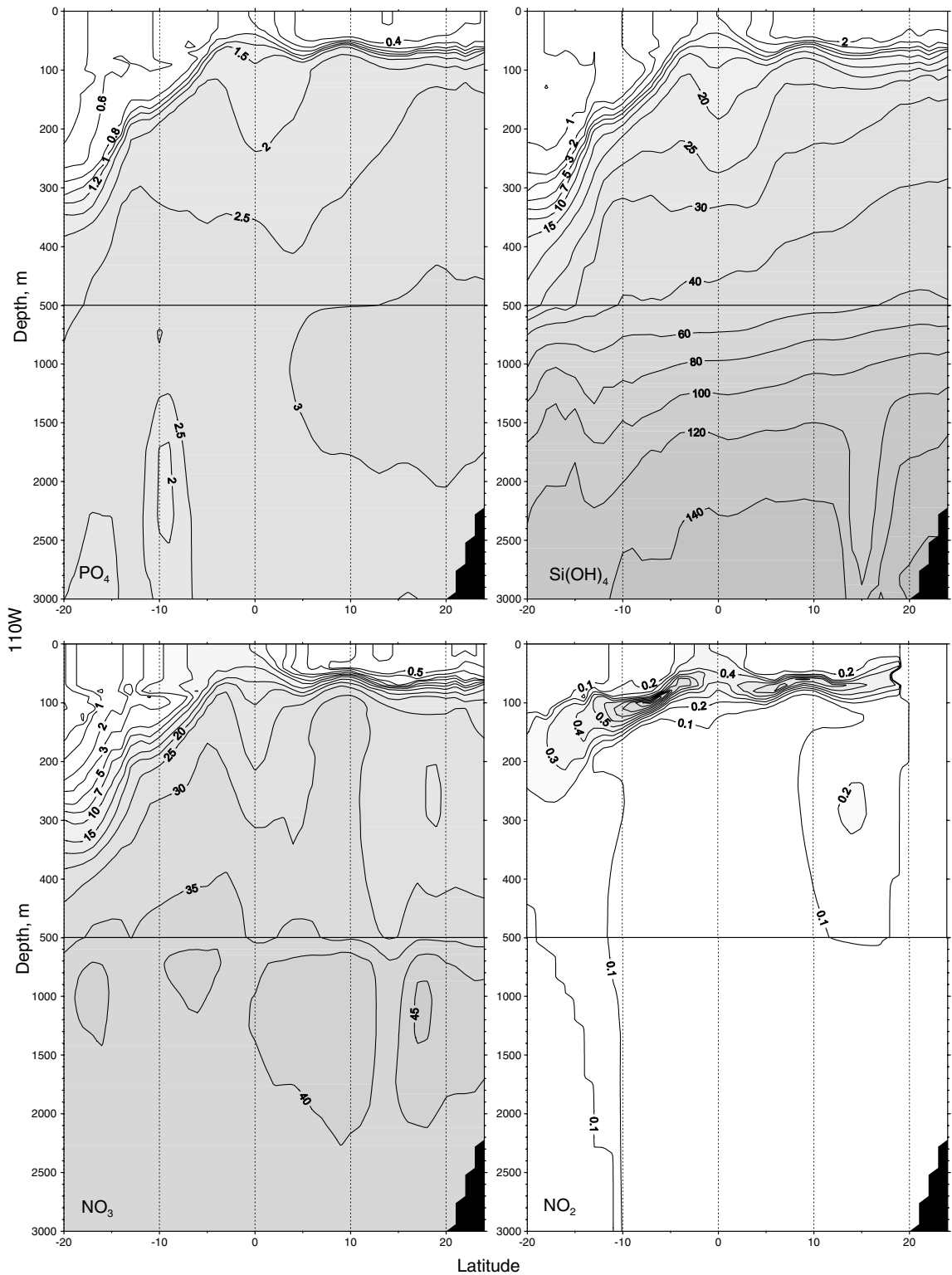


Fig. 15b. Mean meridional sections of nutrients ($\mu\text{mol kg}^{-1}$) along 110°W from WOD01 bottle data (see Appendix): phosphate (PO_4), silicate (Si(OH)_4), nitrate (NO_3), and nitrite (NO_2).

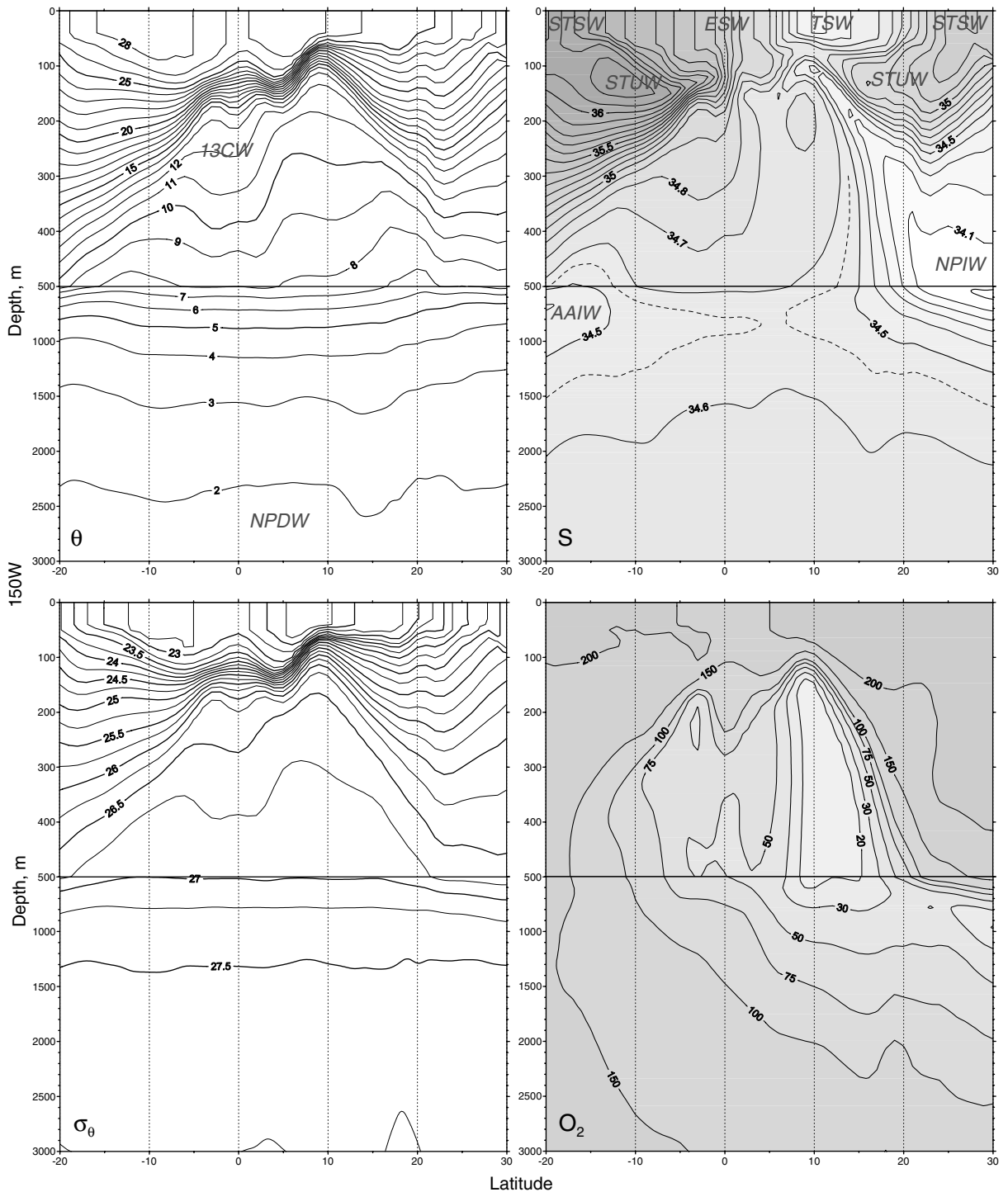


Fig. 16a. Mean meridional sections along 150°W from WOD01 CTD and bottle data (see Appendix): potential temperature (θ , °C, referenced to 0 db), salinity (S), potential density (σ_θ , kg m^{-3}), and dissolved oxygen concentration (O_2 , $\mu\text{mol kg}^{-1}$). Water masses: Tropical Surface Water (TSW), Equatorial Surface Water (ESW), Subtropical Surface Water (STSW), Subtropical Underwater (STUW), 13 °C Water (13CW), Antarctic Intermediate Water (AAIW), North Pacific Intermediate Water (NPIW), North Pacific Deep Water (NPDW).

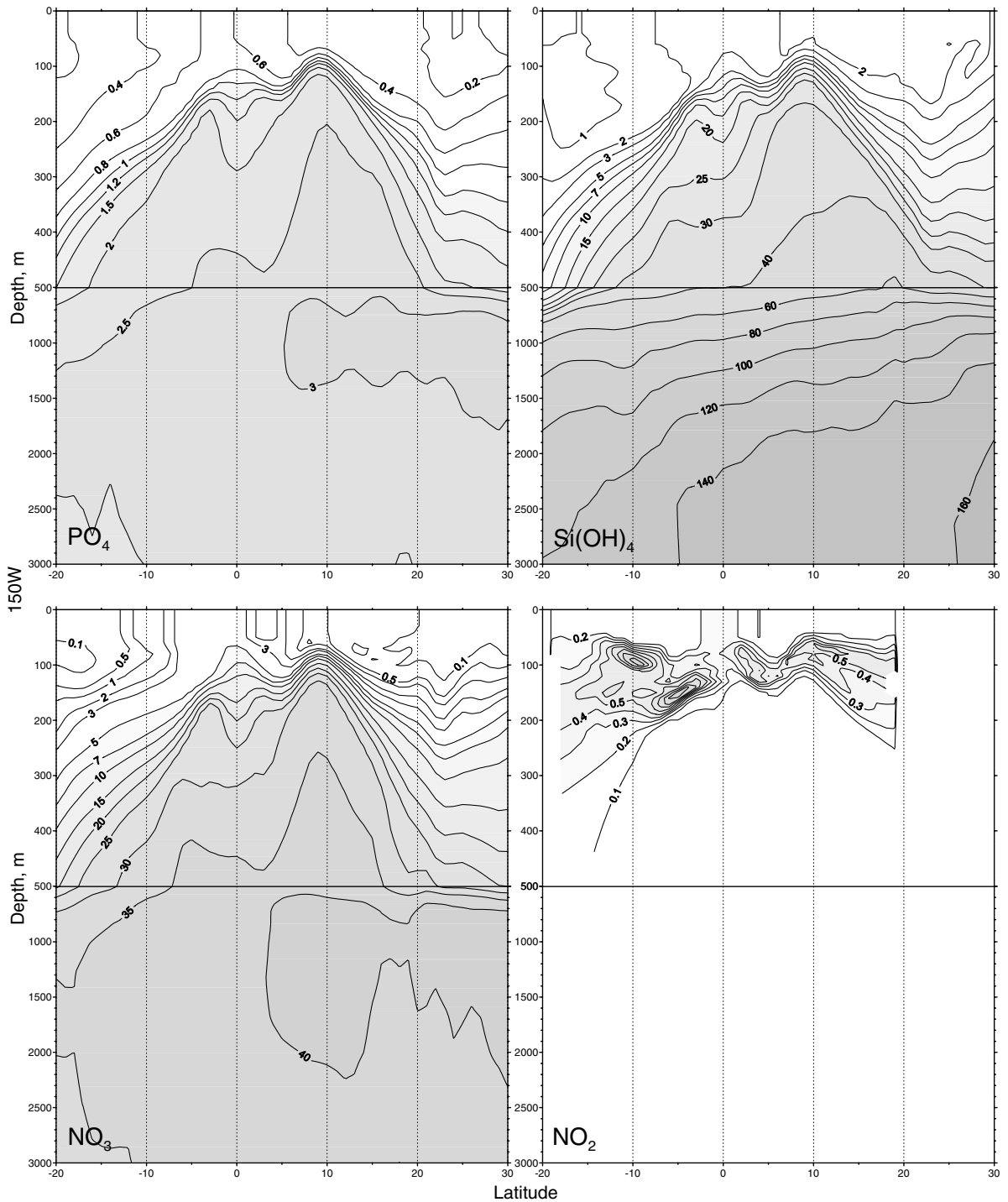


Fig. 16b. Mean meridional sections of nutrients ($\mu\text{mol kg}^{-1}$) along 150°W from WOD01 bottle data (see [Appendix](#)): phosphate (PO_4), silicate (Si(OH)_4), nitrate (NO_3), and nitrite (NO_2).

for large cross-isopycnal flux in the equatorial region and it is now thought that the water in these thermostads originates, at least in part, deeper in the water column (Rowe et al., 2000). The origin of the thermostad structure itself has been attributed to local tropical dynamics, including diffusion associated with the Equatorial

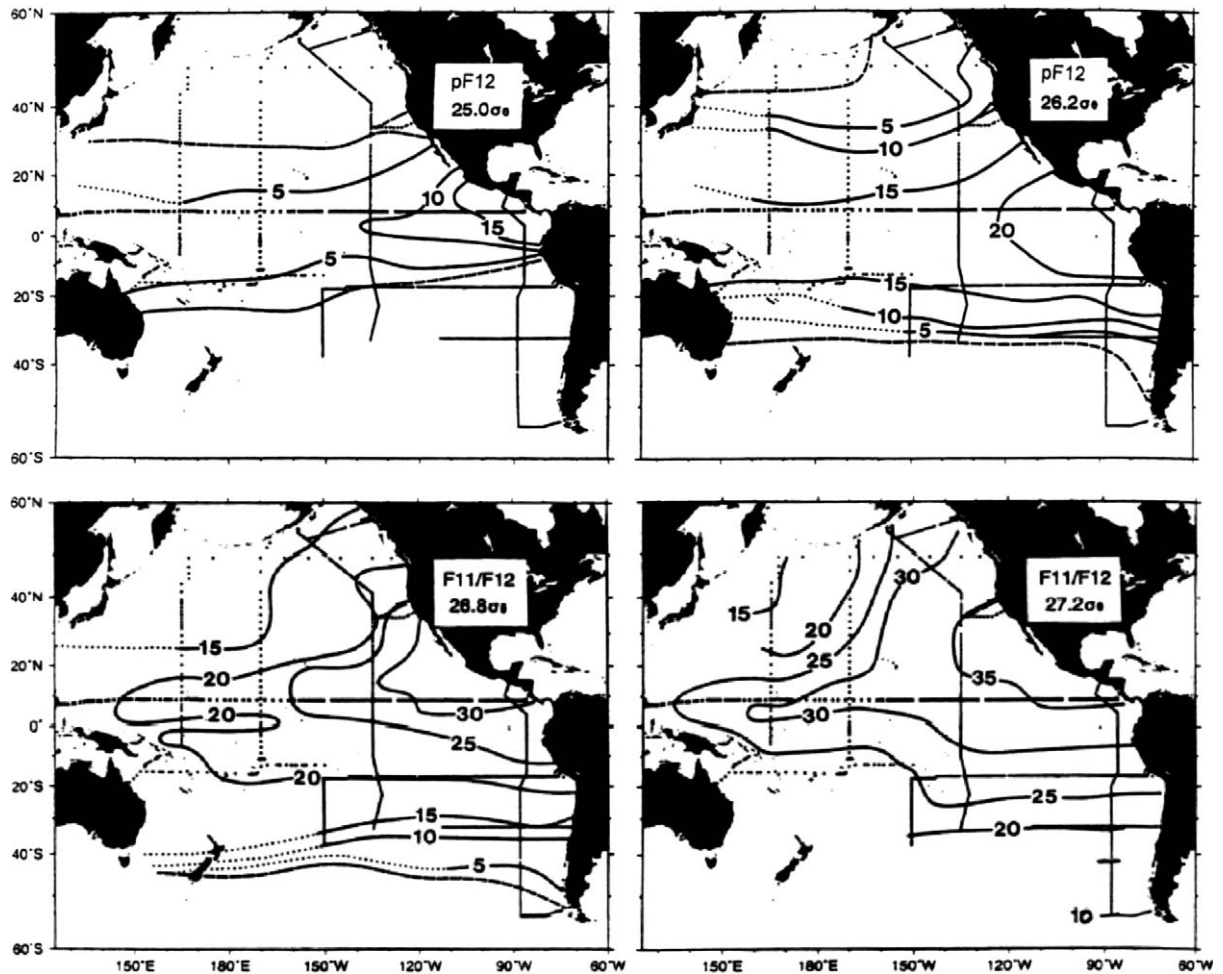


Fig. 17. CFC-derived ages (years) of pycnocline and intermediate waters on four isopycnal surfaces: $25.0\sigma_\theta$ (middle of pycnocline in the eastern tropical Pacific), $26.2\sigma_\theta$ (bottom of pycnocline), $26.8\sigma_\theta$ (~ 500 m), $27.2\sigma_\theta$ (~ 700 m). Adapted with permission of the American Geophysical Union from Fine et al. (2001, Fig. 4).

Undercurrent (McPhaden, 1984), shoaling of the equatorial pycnocline towards the east due to wind forcing (Johnson and Moore, 1997), or ageostrophic circulation akin to the atmosphere's Hadley circulation (Marin et al., 2000), rather than formation as thick layers in the subtropics.

A second thermostad/pycnostad at $4\text{--}13^\circ\text{N}$, north of the 13°C Water and the North Pacific Subsurface Countercurrent and North Equatorial Countercurrent, has been described by some authors in individual sections (135°W , Tsuchiya and Talley, 1996) and is suggested in the 150°W section at $\sim 10^\circ\text{N}$ (Fig. 16, $9\text{--}11^\circ\text{C}$). It is also apparent in the WOCE sections at 105°W and 88°W (Tsuchiya and Talley, 1998; WOCE Pacific Ocean Atlas in Sparrow et al., 2005–2006) Wyrski and Kilonsky (1984) explained this pycnostad at 150°W as the result of mixing of intermediate waters from the north and south. Its zonal persistence in association with the NECC suggests that it is a natural pycnostad of this vigorous westward current.

The broad salinity maximum, extending along 10°N from Costa Rica between 100 and 400 m (Fig. 19), lies between the pycnocline and deeper low-salinity intermediate water beneath Tropical Surface Water in the eastern tropical Pacific. It is clearly separated from STUW to the west by a salinity minimum (NPIW in Fig. 19). Wyrski (1967) identified this salinity maximum as Subtropical Subsurface Water originating as South Pacific Subtropical Surface Water. In contrast, Tsuchiya (1968) described this salinity maximum as originating in the western South Pacific through diapycnal mixing from high-salinity surface waters. The salinity maximum was

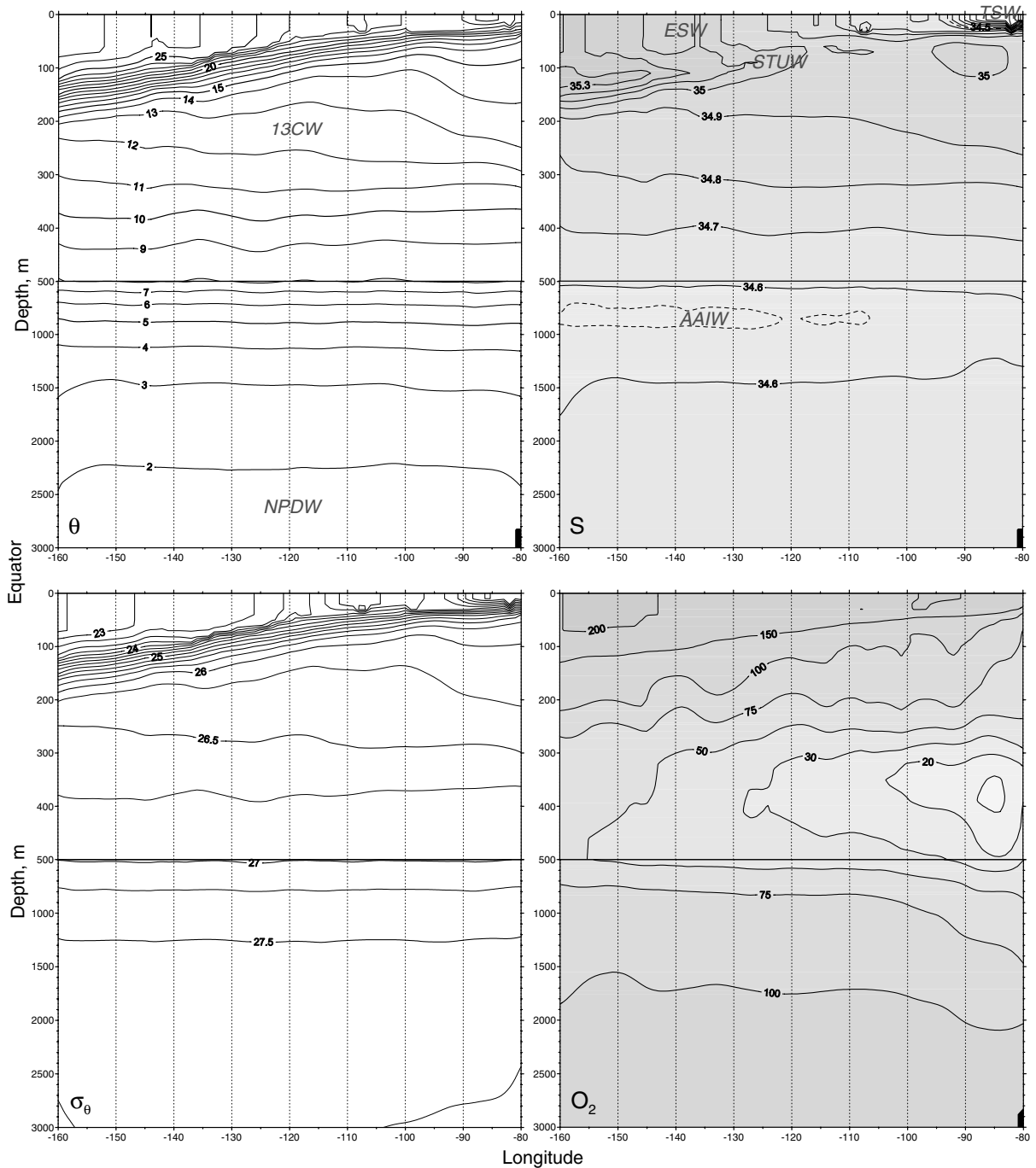


Fig. 18a. Mean zonal sections along the equator from WOD01 CTD and bottle data (see Appendix): potential temperature (θ , °C, referenced to 0 db), salinity (S), potential density (σ_{θ} , kg m^{-3}), and dissolved oxygen concentration (O_2 , $\mu\text{mol kg}^{-1}$). Water masses: Equatorial Surface Water (ESW), Tropical Surface Water (TSW), Subtropical Underwater (STUW), 13 °C Water (13CW), Antarctic Intermediate Water (AAIW), North Pacific Deep Water (NPDW).

called 13 °C Water by Wijffels et al. (1996) because the geographical origin and density of the salinity maximum and the 13 °C Water cores are similar, and because there is no commonly-used water-mass name for the salinity maximum. This interpretation was supported by a recent study (Sloyan et al., 2003) incorporating

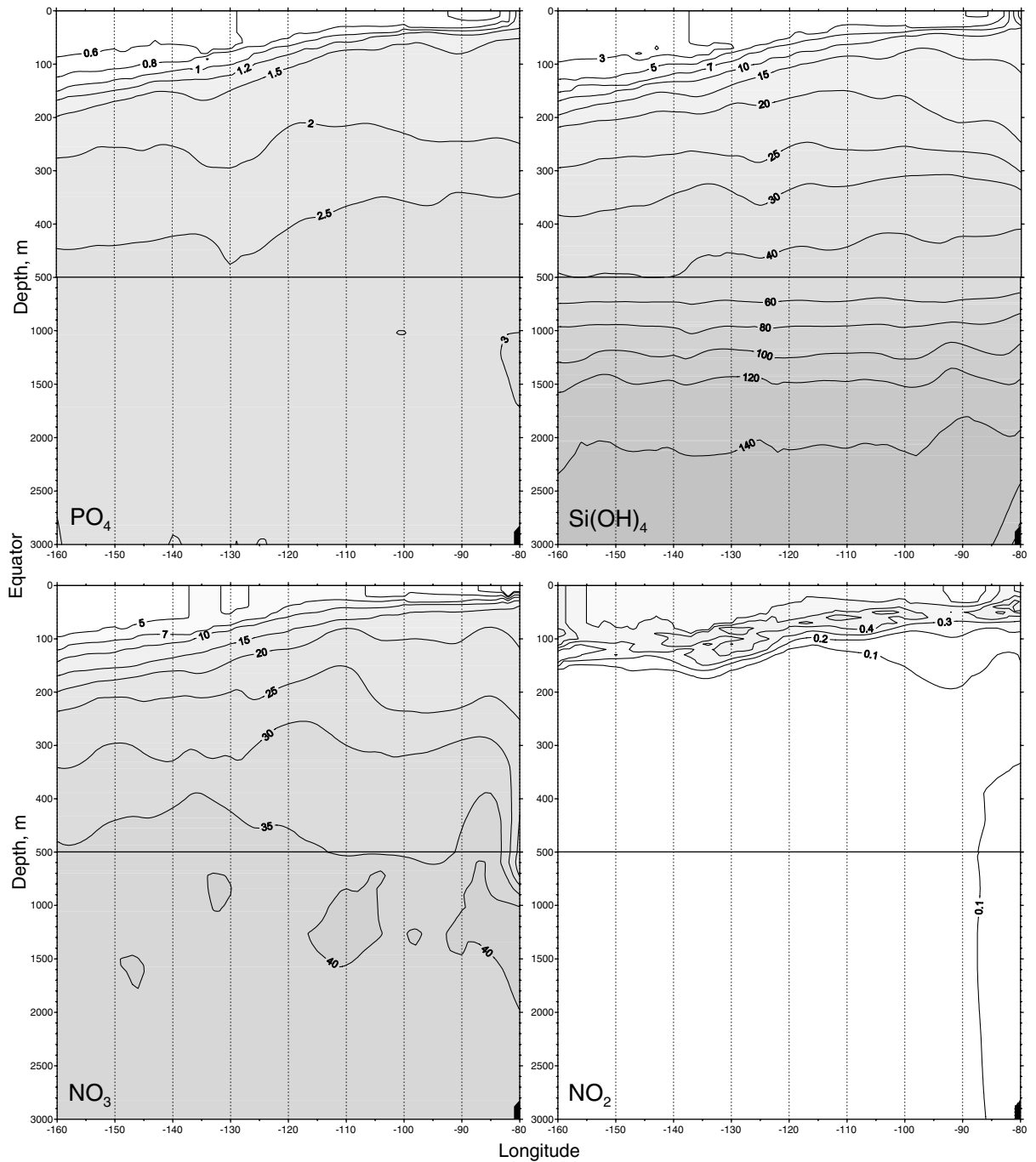


Fig. 18b. Mean zonal sections of nutrients ($\mu\text{mol kg}^{-1}$) along the equator from WOD01 bottle data (see Appendix): phosphate (PO_4), silicate (Si(OH)_4), nitrate (NO_3), and nitrite (NO_2).

numerous observations of hydrography and velocity and showing that this salinity maximum is indeed thermostad water (13CW) that is transported north of the equator as the Northern Subsurface Countercurrent (NSCC) veers north to the east of 100°W . Tsuchiya and Talley (1996) report this large-scale feature and confirm its source in the western South Pacific, but do not give it a water-mass name. We will leave this subpycnocline salinity maximum unnamed, with the understanding that it is essentially modified 13CW.

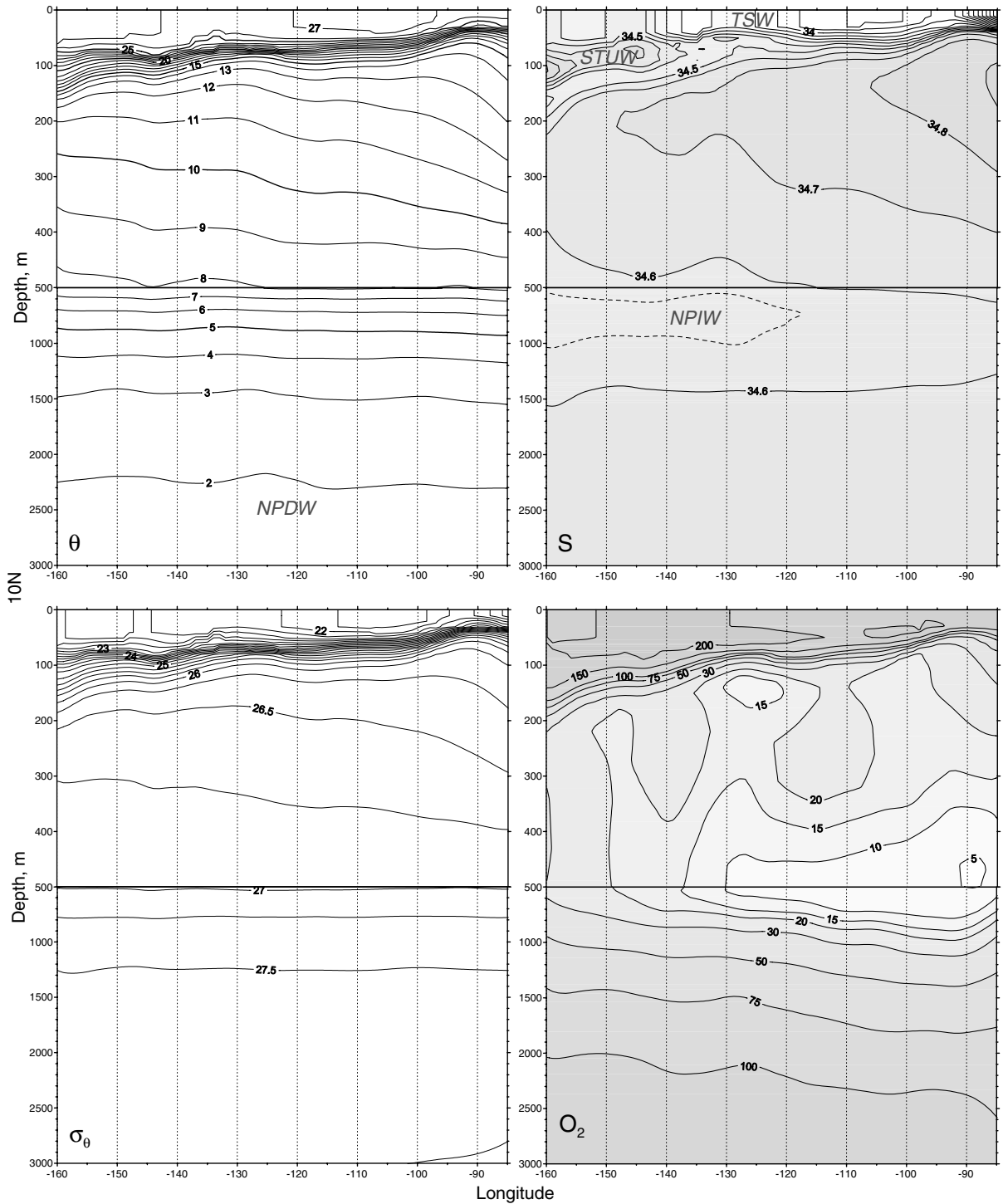


Fig. 19a. Mean zonal sections along 10°N from WOD01 CTD and bottle data (see Appendix): potential temperature (θ , °C, referenced to 0 db), salinity (S), potential density (σ_θ , kg m^{-3}), and dissolved oxygen concentration (O_2 , $\mu\text{mol kg}^{-1}$). Water masses: Tropical Surface Water (TSW), Subtropical Underwater (STUW), Northeast Pacific Intermediate Water (NEPIW), North Pacific Intermediate Water (NPIW), North Pacific Deep Water (NPDW).

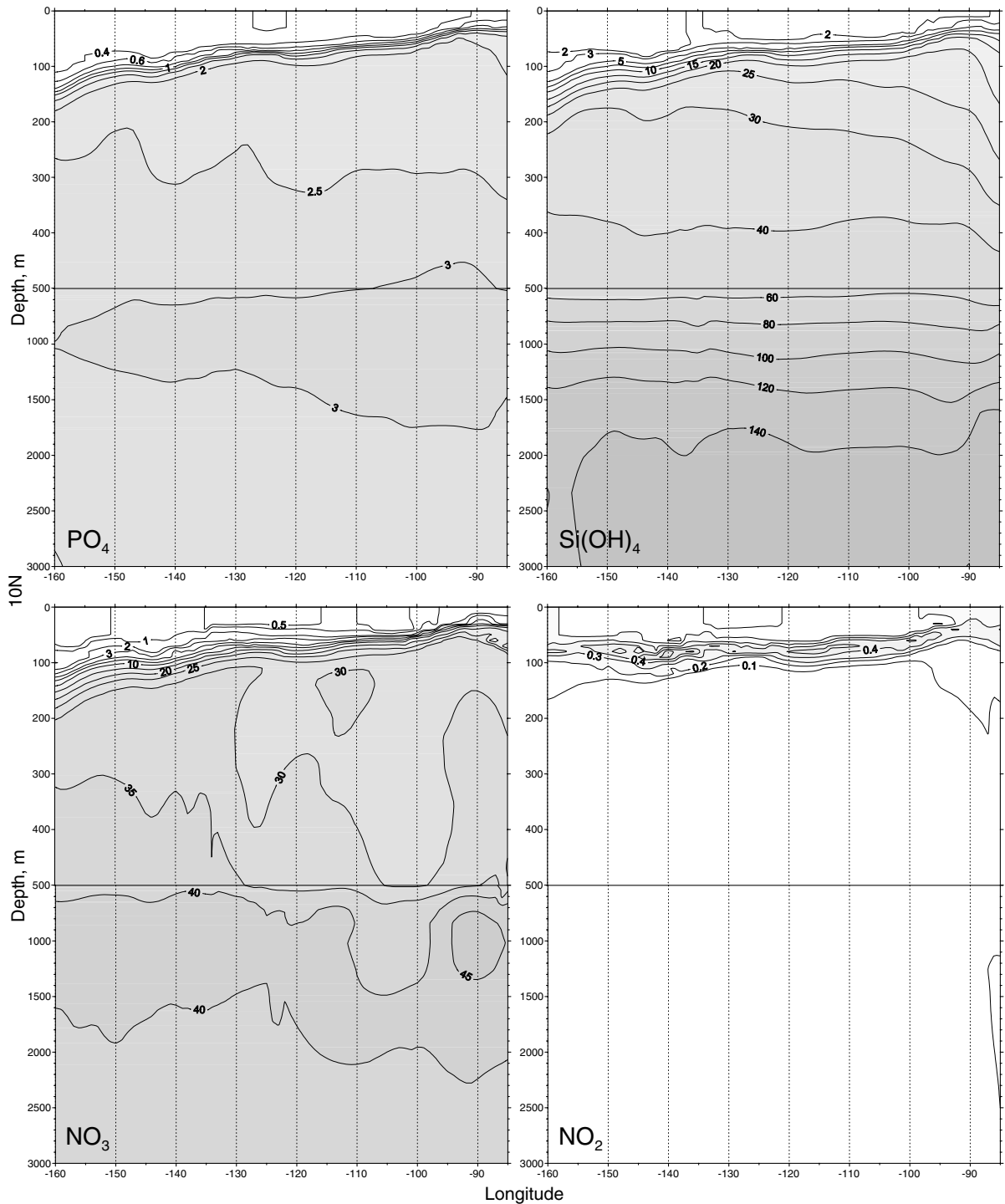


Fig. 19b. Mean zonal sections of nutrients ($\mu\text{mol kg}^{-1}$) along 10°N from WOD01 bottle data (see Appendix): phosphate (PO_4), silicate (Si(OH)_4), nitrate (NO_3), and nitrite (NO_2).

The eastern equatorward border of any subtropical gyre is, in theory, a “shadow zone”, that is, an area not effectively ventilated by surface water subducted to thermocline depths within the gyre, because these waters are confined to the anticyclonic gyre circulation by Sverdrup dynamics (Luyten et al., 1983). The increasing

size of shadow zones with depth is apparent in the tracer age maps reproduced in Fig. 17 from Fine et al. (2001). The 25.0 isopycnal is representative of the South Pacific STUW, described above, and is well-ventilated (tracer ages ~ 5 years) across nearly the full width of the subtropical gyre (O'Connor et al., 2002). The 26.2 isopycnal is the core of the equatorial 13 °C thermostat, and ventilates a more restricted tropical region because of its larger eastern shadow zone (Huang and Qiu, 1998).

Low-salinity intermediate (subpycnocline) water masses lie to the north and south of the equatorial and near-equatorial pycnostad waters described above. The low-salinity water ($S < 34.5$, Figs. 14–16) between 500 and 1000 m, south of 10°S, is Antarctic Intermediate Water (AAIW). AAIW is subducted Subantarctic Mode Water, formed from the deep, winter mixed layer north of the Subantarctic Front in the southeast Pacific (McCartney, 1982; Hanawa and Talley, 2001). AAIW spreads equatorward and westward in the Pacific, and through the Drake Passage to the Atlantic, to occupy intermediate depths around the globe in the tropics and southern subtropics. Tsuchiya and Talley (1996) differentiated subtropical and equatorial “types” of AAIW at 135°W; the difference is illustrated by the characteristics of the salinity minima at 20°S (34.4 at 700 m and $27.1\sigma_\theta$) and at the equator (34.54 at 850 m and $27.3\sigma_\theta$) along 150°W (Fig. 16).

North Pacific Intermediate Water (NPIW) is the low-salinity water between 400 and 800 m north of 20°N along 150°W (Fig. 16, also visible north of 12°N along 110°W in Fig. 15). NPIW originates by subsidence in the Okhotsk Sea and at the Oyashio Front in the western North Pacific, with some contribution from the Gulf of Alaska (You, 2003), and is found in the subtropical North Pacific between the Subarctic Front at $\sim 40^\circ\text{N}$ and 15–20°N to about 130°W (Talley, 1993). Thus, it is not a major water mass in the eastern tropical Pacific, found only at the northwest extreme. However, phosphate and nitrate maxima correspond to the NPIW salinity minimum and extend across the equator towards the AAIW in the southern hemisphere (Figs. 14b, 15b and 16b).

Shallow salinity minima in the tropical Pacific are often seen in individual sections between the Subtropical Underwater salinity maxima and the Intermediate Water salinity minima. These waters originate from low-salinity surface waters at high latitudes, including subarctic or subantarctic waters in eastern boundary currents (Reid, 1973; Yuan and Talley, 1992). The thin salinity minimum at 100 m depth near 10°N at 150°W (Fig. 16) appears to be the shallow salinity minimum originating in the California Current (Reid, 1973; also seen in Fig. 2 of Wyrтки and Kilonsky, 1984), although it is not differentiated from the deeper NPIW salinity minimum in this mean section. This shallow salinity minimum was called Northeast Pacific Intermediate Water by Wijffels et al. (1996) to reflect its origins, although Tsuchiya (1968) refers to it as California Current Water. Yuan and Talley (1992) showed that this shallow tropical salinity minimum is not a distinct water mass, but results from splitting of the overall salinity minimum formed by NPIW and California Current Water by the salinity maximum of STUW from the South Pacific. They referred to the resulting upper minimum as the tropical salinity minimum. It is clearly seen in the mean 10°N section (Fig. 19a) west of 135°W. It is at 90 m depth at 135°W and 160 m depth at 160°W, centered on the 13 °C isotherm and $25.8\sigma_0$ isopycnal; in the WOCE 10°N section, it deepens to about 250 m in the far western Pacific (Wijffels et al., 1996). In contrast, the NPIW salinity minimum is centered on the 6 °C isotherm and $27.2\sigma_0$ isopycnal in this section.

Zonal sections along the equator (Fig. 18) and 10°N (Fig. 19) show the surface, pycnocline, and intermediate water masses described above. The westward deepening of the thermocline set up by the trade winds (Wyrтки, 1975b) is more pronounced along the equator than along 10°N. However, the thermocline along 10°N is stronger and shows local peaks at 126°W and 90°W (Costa Rica Dome, Fig. 9a). The patterns of oxygen and nutrients in the meridional and zonal sections will be discussed below.

Sverdrup et al. (1942) labeled the subpycnocline waters between 8 and 15 °C in the tropical Pacific, below the salinity maximum of what is now called the Subtropical Underwater, as “Equatorial Water”. This “water mass” was named to differentiate it from Central Waters, which are subducted in the subtropical convergences and comprise the entire broad thermocline in the subtropical gyres. Equatorial and Central Waters correspond to the linear T–S relation below the salinity maxima (see Fig. 23). Although some textbooks have retained this nomenclature (Pickard and Emery, 1990; Tomczak and Godfrey, 2001), we do not use “Equatorial Water” here because it does not indicate the sources of the waters in the various layers that are lumped under that name (e.g. Subtropical Underwater, 13 °C Water, Eastern Subtropical Mode Water, shallow salinity minima; Johnson and McPhaden, 1999).

6. Oxygen minimum layer

Eastern tropical Pacific subpycnocline waters are very low in oxygen (Fig. 20). In the world ocean, deep waters of the eastern North Pacific and northern Indian Ocean are low in oxygen (Fig. 21). However, the eastern tropical Pacific oxygen minimum layer, lying between the pycnocline and intermediate waters, is remarkable for its size and degree of hypoxia (Kamykowski and Zentara, 1990). The large and thick oxygen minimum in the subarctic North Pacific is deeper and less depleted (Fig. 21) and is clearly the result of lack of ventilation since no deep water is formed in the North Pacific. Reid (1981) presents global maps of properties on an arbitrary deep isopycnal surface (potential density relative to 2000 decibars $\sigma_2 = 37.0$, at a depth of 2200–2600 m in the Pacific north of the Antarctic Convergence): a distinct oxygen minimum, with corresponding phosphate and silicate maxima, is seen both in the eastern subarctic Pacific and in the Arabian Sea, but not in the eastern tropical Pacific where this deep isopycnal is below the oxygen minimum layer. In the analysis of World Ocean Atlas climatological fields illustrated in Fig. 21, the eastern tropical Pacific oxygen minimum is on an isopycnal surface of $\sigma_\theta = 26.7$ – 27.0 , while the eastern subarctic Pacific oxygen minimum is on an isopycnal surface of $\sigma_\theta = 27.3$ – 27.5 (not shown). Thus, the shallow eastern tropical Pacific oxygen minimum is distinct from the deep subarctic Pacific oxygen minimum and other factors must be considered to explain it.

Richards (1957) reviewed the early debate between dynamic (physical) and biological explanations of oxygen minima at “intermediate depths”, but it is now generally accepted that both factors are involved. Brandhorst (1959) stated that “depletion of oxygen is accentuated in areas where there is both a highly productive, photosynthetic layer and a strong thermocline which impedes convection and exchange of water richer in oxygen from above”, emphasizing vertical transport in an analysis of limited data from the eastern tropical Pacific. Sarmiento et al. (1988) analyzed the “causes of anoxia” in deep water of the open ocean as a balance between circulation (the supply of oxygen from high-latitude surface water) and production (the rain of oxidizable particulates from local surface water). The extreme oxygen deficiency in the eastern tropical Pacific oxygen minimum zone is attributable to several factors: (1) high phytoplankton production at the surface; (2) a sharp permanent pycnocline that prevents local ventilation of subsurface waters; (3) a sluggish and convoluted deep circulation and therefore old “age” of subpycnocline waters (see Fig. 17). Lowest oxygen concentrations are found beneath the Peru Current off northern Peru, south of the equator, and beneath the eastern Pacific warm pool off the coast of SW Mexico (Fig. 20). Oxygen minimum concentrations are lower north of the equator because there is no source of oxygen-saturated, high-density water at the surface in the North Pacific (Reid, 1973). In vertical sections (Figs. 14a, 15a and 16a), the oxygen minima lie beneath the high-salinity subtropical subsurface waters of the pycnocline, subducted from the surface at midlatitudes, and above the low-salinity intermediate waters subducted from the surface at higher latitudes. At these subpycnocline depths, there are no direct interior pathways from subtropical ventilation regions towards the equator in the North or South Pacific and oxygenated water subducted from the surface must come from the west in the subsurface countercurrents (Johnson and McPhaden, 1999). Oxygen concentrations are higher in the oxygen minimum along the equator due to the more rapid transport of oxygenated water from the western Pacific in the EUC (Tsuchiya et al., 1989; Lukas, 1986).

Wyrski (1962) showed that vertical oxygen minima can result from exponentially decreasing rates of oxygen consumption with depth and no horizontal advection of oxygen. Although this vertical advection-eddy diffusion model was an oversimplification, it did show that both in situ oxygen consumption by biological processes and physical transport are required to account for an oxygen minimum layer at intermediate depths (Kester, 1975). Riley (1941) completed a mathematical analysis of physical and biological factors that determine the distribution of nonconservative properties in the Atlantic. He concluded that 90% of organic matter produced by phytoplankton is utilized in the upper 200 m and that the remainder sinks to deeper waters where respiration and bacterial decomposition result in oxygen consumption. Consistent with the eastern tropical Pacific oxygen minimum layer, Riley also showed that an oxygen minimum can be formed between depths below the productive surface layer where biological oxygen consumption is highest and intermediate depths where replenishment by advection/diffusion is lowest.

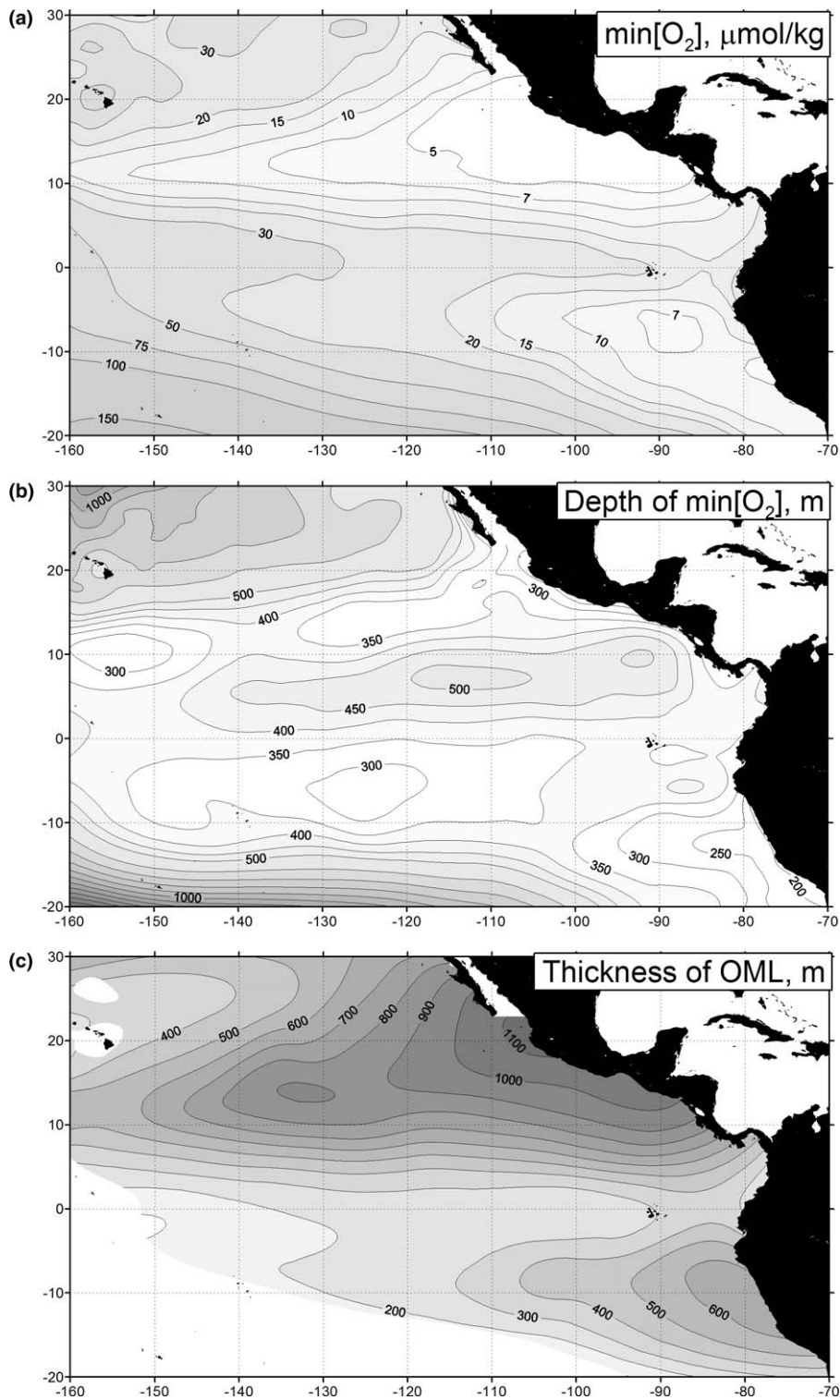


Fig. 20. Eastern tropical Pacific oxygen minimum layer from WOD01 CTD and bottle data (see Appendix): (a) minimum dissolved oxygen concentration ($\mu\text{mol kg}^{-1}$); (b) depth of minimum oxygen concentration; (c) thickness of oxygen minimum layer ($<45 \mu\text{mol kg}^{-1}$).

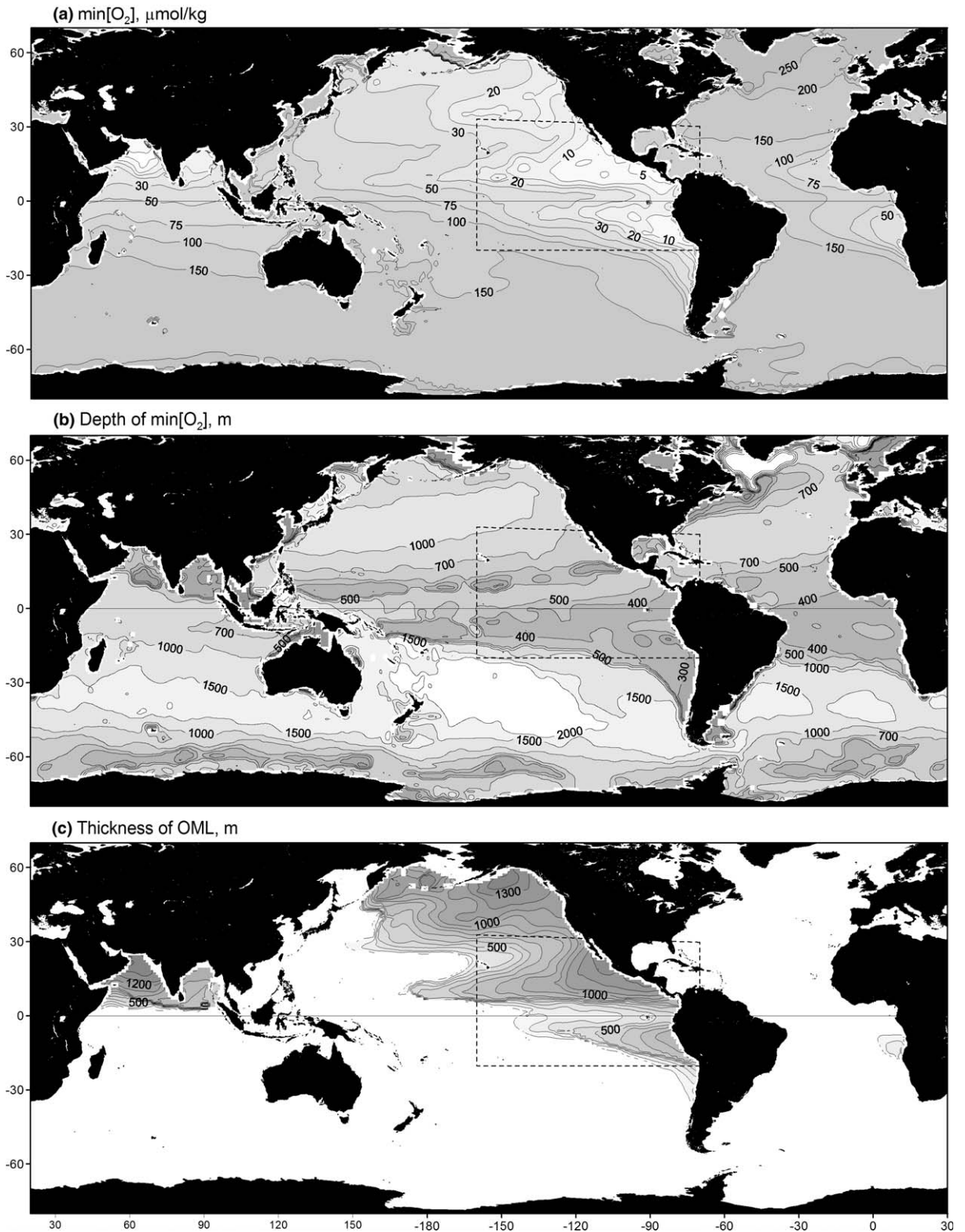


Fig. 21. Global oxygen minimum layer from World Ocean Atlas 2001 gridded fields at standard depths (see [Appendix](#)): (a) minimum dissolved oxygen concentration ($\mu\text{mol kg}^{-1}$); (b) depth of minimum oxygen concentration; (c) thickness of oxygen minimum layer ($<45 \mu\text{mol kg}^{-1}$). Rectangle marks extent of [Fig. 20](#).

7. Nutrients

The strong thermocline/pycnocline of the eastern tropical Pacific is also a strong nutricline (Fig. 19). Relationships between temperature and nutrient concentrations have been demonstrated both globally (Kamykowski and Zentara, 1986) and for the eastern tropical Pacific (Zentara and Kamykowski, 1977; Chavez et al., 1996). Regional and temporal differences in temperature–nutrient relationships are affected by processes of biological uptake and remineralization, as well as surface heat flux, advection, and vertical mixing (Chavez et al., 1996). The nitrate–temperature relationship for eastern tropical Pacific waters (Fig. 22) shows the non-linearity reflecting the influence of phytoplankton uptake in surface waters ($T > 15$ °C) and remineralization in deeper waters. The nitrate maximum at 4–5 °C corresponds to relatively “old” water at the base of the oxygen minimum layer. Consequences of the shallow but strong eastern tropical Pacific nutricline for phytoplankton production, and the significance of the low but not depleted nutrient content of Equatorial Surface Water, are reviewed in Pennington et al. (2006).

A consistent pattern in all the vertical sections is that nitrate and phosphate increase with depth to about 500 m, with a slight maximum at intermediate depths of 500–1500 m, while silicate continues to increase with depth. This pattern reflects differences in remineralization processes (Jiang et al., 2003).

The nitrate–phosphate relationship for eastern tropical Pacific waters (Fig. 22a) has a slope of 14.0 and a positive x -intercept of $0.21 \mu\text{mol kg}^{-1} \text{PO}_4$. The N:P slope is consistent with a value of 14.1, slightly less than the Redfield ratio of 16, in a global dataset (Tyrrell and Law, 1997). However, there is no subset of data points with a secondary trend at a low N:P ratio of ~ 2 that these authors interpreted as indicating denitrification. The positive x -intercept reflects the global predominance of nitrate limitation, although there is increasing evidence of N_2 fixation and resultant phosphate limitation in the North Pacific subtropical gyre (Karl, 1999).

A nitrite maximum occurs in the lower thermocline/nitracline throughout the world ocean (Figs. 14b, 15b, 16b, 18b and 19b). Nitrite is important in the global ocean as a nitrogen cycle intermediary. The primary nitrite maximum in the lower euphotic zone generally results from excretion by phytoplankton and/or nitrification of ammonium by chemoautotrophic bacteria (Dore and Karl, 1996). A deep nitrite maximum below

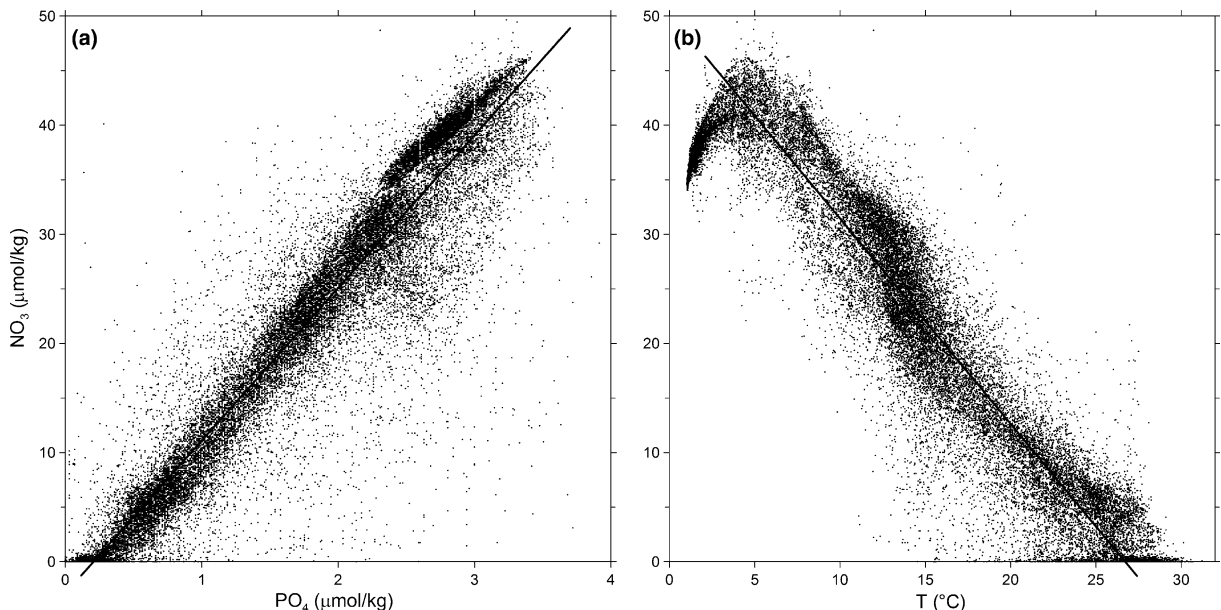


Fig. 22. Nutrient relationships in WOD01 bottle data (see Appendix) from stations in tropical and equatorial waters of the eastern tropical Pacific (10°S – 20°N out to 140°W , $n = 2219$). (a) Nitrate and phosphate, $n = 32,954$. Regression line is $[\text{NO}_3] = 14.0 [\text{PO}_4] - 2.98$. (b) Nitrate and temperature, $n = 30,100$. Linear regression for $T > 5$ °C has an x -intercept at 26.7 °C. Separate regressions for tropical and equatorial waters were not significantly different.

the primary maximum, resulting from reduction of nitrate by denitrifying bacteria, has been detected in the oxygen minimum zone at stations in the eastern tropical North Pacific (Brandhorst, 1959; Thomas, 1966; Cline and Richards, 1972). This secondary nitrite maximum is visible at some locations in the eastern meridional mean sections (11°S along 88°W in Fig. 14b, 14°N along 110°W in Fig. 15b).

8. Deep and bottom waters

Properties of deep and bottom waters in the Pacific are set by their distant sources in the Antarctic and North Atlantic, with modification through diapycnal processes, oxygen consumption and nutrient regeneration, and by the complicated basin geometry (Tsuchiya and Talley, 1996). North Pacific Deep Water (NPDW) is the 1.2–2 °C water deeper than ~2500 m in the sections shown here (Wijffels et al., 1996; Johnson and Toole, 1993). NPDW is marked by a broad silicate maximum extending from the north in deep sections (Tsuchiya and Talley, 1996). The upper edge of this silicate maximum is seen in the 0–3000 m sections presented here (Figs. 14b, 15b and 16b). The deep water (roughly 1500–2500 m or down to the ridge tops) differs from South Pacific deep waters at the same density in having significantly higher nutrients and lower oxygen (Reid, 1997; Tsuchiya and Talley, 1998). This indicates that the tropical deep waters are older and dynamically separated from South Pacific subtropical deep waters, with a broad transition region at 15–25°S. Direct connection between the subtropical and tropical deep waters occurs in the western Pacific (Reid, 1997).

Within the tropical deep waters, most properties, and especially ΔHe_3 originating from hydrothermal venting at the mid-ocean ridges, show a structure consisting of two wide westward-extending plumes centered at 2500 m depth and about 10°N and 10°S, separated by an eastward-extending plume close to the equator (Östlund et al., 1987; Talley and Johnson, 1994). Deep water at the equator is markedly lower in ΔHe_3 and is slightly cooler and saltier, lower in nutrients, and higher in oxygen than the broad off-equatorial plumes. In the vertical, the eastern tropical Pacific deep waters are not clearly differentiated from the pycnocline waters in terms of nutrients and oxygen, since the vertical oxygen minimum and nutrient maxima are located in the upper ocean in the eastern tropical Pacific, due to enhanced biological productivity.

Bottom water (>4000 m) in the Pacific is Lower Circumpolar Water (LCPW), a mixture of Antarctic Bottom Water formed in the Weddell Sea and North Atlantic Deep Water formed in the northern North Atlantic. LCPW in the eastern tropical Pacific north of the equator is characterized by relatively high oxygen and low silicate concentrations (Wijffels et al., 1996). LCPW flows into the eastern tropical Pacific from the Northeast Pacific Basin on the western flank of the East Pacific Rise (105–110°W, see Fig. 3 of Fiedler and Lavín, 2006), at the end of a circuitous path in a northward deep western boundary current through the Central Pacific Basin and then an eastward branch between the Hawaiian and Line Islands (Johnson and Toole, 1993).

Bottom waters in the deep basins of the eastern tropical Pacific are somewhat isolated from direct input of LCPW and their characteristics are modified. The three main basins are the Guatemala, Panama, and Peru Basins, separated by the Cocos Ridge and the Carnegie Ridge, respectively (Fiedler and Lavín, 2006, Fig. 3). Abyssal properties in the eastern tropical Pacific are summarized from the property descriptions for the WOCE section at 88°W (Tsuchiya and Talley, 1998) and isopycnal maps of the Pacific in Reid (1997). Bottom waters in the Peru Basin enter from the south from the Chile Basin through several gaps in the ridges and in the Peru–Chile Trench. Oxygen is higher and nutrients are lower in the abyssal waters than in the overlying deep waters, with changes from south to north indicating aging (lower oxygen and higher nutrients to the north). The Panama Basin straddles the equator and is shallower overall than the Peru or Guatemala Basins. Its bottom waters originate from the Peru Basin to the south, through a gap between the South American coast and Carnegie Ridge (Laird, 1971). Active geothermal processes in the basin increase the temperature of the bottom waters slightly (Laird, 1971; Lonsdale, 1976). The source of abyssal waters in the Guatemala Basin is north of the equator, as reflected in its bottom waters being colder, more saline, and denser than the bottom waters of the Panama Basin, which sits directly to the south. The Guatemala Basin waters are slightly older, as measured in lower oxygen, than its source waters west of the East Pacific Rise, and appear to be modified slightly through geothermal heating or downward diffusion of heat (Wijffels et al., 1996). Waters in the deep Middle America Trench are homogeneous below 3800 m and originate from the bottom waters of the (shallower) Guatemala Basin.

9. Summary

The hydrography of the eastern tropical Pacific is summarized briefly below and in Fig. 23. We have tried to follow the modern definition of “water mass” as having a single source at the surface (or a mixture of two such sources) and to present a consensus from the reviewed literature, although there is not, and may never be, a universally accepted water mass terminology.

The eastern Pacific warm pool is the central surface feature of the eastern tropical Pacific, with warm, low-salinity Tropical Surface Water over a shallow and strong pycnocline; seasonal and ENSO variability are relatively low. The equatorial cold tongue is cool, moderate-salinity Equatorial Surface Water over a shallow but relatively weak pycnocline; seasonal and ENSO variability are relatively high. Cool, low-salinity eastern boundary current waters flow into the eastern tropical Pacific from the north and south. Warm, high-salinity subtropical surface waters flow into the eastern tropical Pacific as Subtropical Underwater after being subducted into the thermocline primarily in the southern Subtropical Convergence. The pycnocline in the eastern tropical Pacific is a thermocline reinforced by a halocline and is uniquely shallow and strong.

Upwelling of thermocline waters into the surface layer is evidenced by relatively cool surface temperatures, high salinity and high nutrient concentrations along the equator, coastal Peru and Baja California, and at the

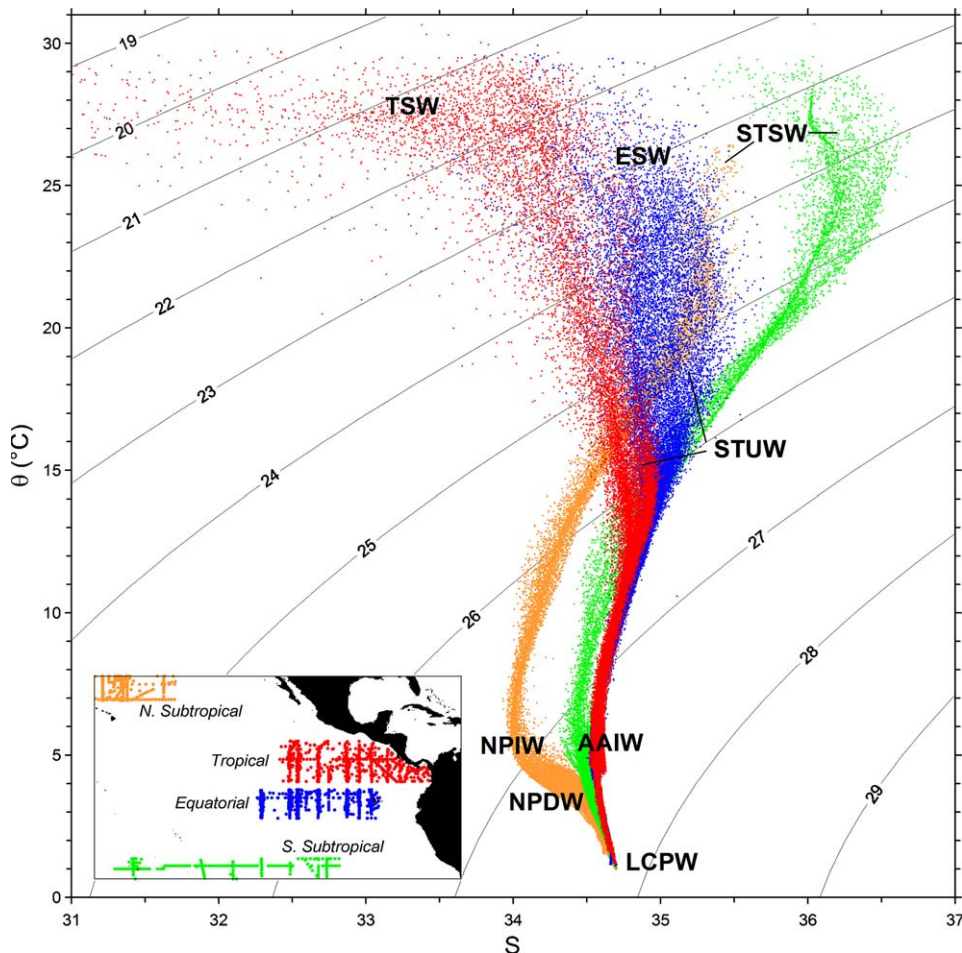


Fig. 23. θ - S diagram of water masses in four selected regions of the eastern tropical Pacific, from WOD01 CTD data (see Appendix): Tropical Surface Water (TSW), Equatorial Surface Water (ESW), Subtropical Surface Water (STSW), Subtropical Underwater (STUW), Antarctic Intermediate Water (AAIW), North Pacific Intermediate Water (NPIW), North Pacific Deep Water (NPDW), and Lower Circumpolar Water (LCPW). Potential density contours in units of kg m^{-3} .

Costa Rica Dome. Thermocline waters are upwelled and mixed into the surface layer by winter wind jets at the Gulfs of Tehuantepec, Papagayo, and Panama. Nutrient-rich thermocline waters lie close to the surface along the countercurrent thermocline ridge between the North Equatorial Countercurrent and the North Equatorial Current.

A high-salinity subpycnocline water mass beneath the eastern Pacific warm pool is modified 13 °C Water that originates in the western South Pacific and crosses the basin equatorward of the North and South Sub-surface Equatorial Countercurrents. Low-salinity Intermediate waters enter the eastern tropical Pacific beneath the pycnocline from both the north (North Pacific Intermediate Water) and south (Antarctic Intermediate Water). Subpycnocline waters in the eastern tropical Pacific are depleted of oxygen, with the greatest depletion below the strong pycnocline of the eastern Pacific warm pool, where ventilation by intermediate water through a long and convoluted path is low and biological productivity is high near the coast. Deep and bottom waters in the eastern tropical Pacific are relatively homogeneous and are formed in the Antarctic and North Atlantic.

Acknowledgements

We thank Miguel Lavín and Billy Kessler for helpful comments on an early version of this paper, as well as two anonymous reviewers. This is a contribution to the scientific agenda of the Eastern Pacific Consortium of the InterAmerican Institute for Global Change Research. Support was also provided by the Protected Resources Division of NOAA Fisheries, Southwest Fisheries Science Center.

Appendix. Methods

CTD, XBT, MBT, bottle and surface data were obtained from the World Ocean Database 2001 (WOD01; Conkright et al., 2002a). Data files updated as of 30 August 2003 were used. The few observations prior to 1950, primarily bottle and MBT samples, were not utilized. Data values were used if all quality flags associated with the values indicated an acceptable value. The only further screening was omission of salinity values < 28 or > 37 . Ocean Data View (Schlitzer, 2002) was used to read the WOD01 data files into a collection, eliminate stations apparently on land, calculate potential temperature and density (reference level = 0), and write the collection data to a text file for further analysis. Percent oxygen saturation was calculated according to Weiss (1970). The thermocline was characterized for BT and CTD temperature profiles by finding the depth interval with maximum temperature gradient $\Delta T/\Delta z$, with $\Delta T > 2$ °C or $\Delta z > 10$ m; thermocline depth is the midpoint of that interval and thermocline strength is the value of the gradient. Mixed layer depth was calculated from individual BT and CTD profiles as the depth at which temperature was 0.2 °C less than the temperature at 10 m depth (De Boyer Montégut et al., 2004).

Thermocline depth in the tropical ocean is conventionally indexed by the depth of the 20 °C isotherm (Kessler, 1990). Recently, Wang et al. (2000) proposed using a “representative” isotherm equal to the average of the local annual mean surface temperature and 12 °C (representing the temperature at the base of the thermocline) as a valid index throughout the tropical Pacific, including the cold tongue and eastern boundary current waters. We found that neither of these isotherm indices fully captured the seasonal thermocline in the subtropics and, therefore, prefer the maximum temperature gradient criterion as described above. Temperature at the thermocline depth was 19–21 °C throughout most of the study area between 10°S and 20°N, including the equatorial cold tongue, but was ≥ 22 °C in the eastern Pacific warm pool and ≤ 17 °C in Peru Current waters and in California Current waters between Baja California and 135°W.

Objective analysis of horizontal or vertical (section) fields was performed by the ocean interpolation algorithm of Ridgeway et al. (2002): loess-weighted observations are projected onto quadratic functions of spatial coordinates while simultaneously fitting annual and semiannual harmonics, and the Southern Oscillation Index (SOI) to account for interannual variability. Quarterly deviations are calculated from the annual and semiannual harmonics. The magnitude of the seasonal cycle is represented by the sum of the annual and semiannual amplitudes. Although this sum is not equivalent to an annual range, because of the phasing of the two harmonics, the annual harmonic was typically dominant and the sum of amplitudes represents a rough but convenient measure of within-year variability. ENSO variability is the variance accounted for by the linear

fit to SOI. The “ENSO Effect” is presented as -2 times the fit to SOI, representing the effect of a typical El Niño event. Unlike Ridgeway et al. (2002), fitting in the vertical dimension was isopycnal rather than isobaric, to preserve sharp gradients in the pycnocline (Johnson et al., 2002). To account for anisotropy, the spatial coordinates were linear transforms of latitude ($1\times$), longitude ($0.67\times$), and potential density (σ_θ , $20\times$).

Sample sizes and fitting parameters for the gridding of horizontal fields are summarized in Table 1. At each grid point, all observations within a minimum search radius (d_{\min}) were selected. If the number of observations was less than n_{\min} , the search radius was expanded until sufficient observations were selected; d_{\max} is the maximum search radius needed to select n_{\min} observations. The search radius was not allowed to expand beyond a distance equivalent to 20° latitude, so that for some grid points in the nutrient and oxygen fields, n_{\min} observations could not be obtained. In general, search radius exceeded d_{\min} in regions of low sample density in the SW of the study area, and the number of observations within d_{\min} exceeded n_{\min} in northern and coastal regions of high sample density in the study area (Fig. 1). Loess-weighted regression was performed on the selected observations at each grid point, as described above. The ranges of variance explained are listed in Table 1.

World Ocean Atlas 2001 (WOA01) one-degree objectively analyzed mean annual fields were mapped to provide a global context for the eastern tropical Pacific horizontal fields (Conkright et al., 2002b, which is <http://www.nodc.noaa.gov/OC5/WOA01/wao1dat.html>). WOA01 values are at 33 standard depths (0, 10, 20, 30, 50, 75, 100, 125, 150, 200, 250, 300, 400, 500, 600, 700, 800, 900, 1000, 1100, 1200, 1300, 1400, 1500, 1750, 2000, 2500, 3000, 3500, 4000, 4500, 5000 and 5500 m). Surface temperature and salinity (Fig. 6) are the 0 m standard depth values. Vertical structure parameters related to the oxygen minimum layer (Fig. 21) were calculated with the same algorithms used for WOD01 station profiles, except that profiles were derived by spline interpolation of the WOA01 standard depth values. Barrier layer thickness was calculated as in Sprintall and Tomczak (1992), from spline-interpolated WOA01 temperature and salinity profiles, as the difference between the isothermal layer depth (where $T - T_0 = -0.5^\circ\text{C}$) and the mixed layer depth. Mixed layer depth based on change in potential density was calculated with a variable σ_t criterion, as the depth where σ_t equals the sea surface σ_t plus an increment in σ_t equivalent to $\Delta T = -0.5$ (Fofonoff, 1985).

Vertical structure parameters related to the pycnocline (Fig. 7) were derived from σ_θ values at standard depths, calculated from potential temperature and salinity values relative to 0 m (Fofonoff, 1985), with an extension of the mixed layer depth algorithm of Polovina et al. (1995). The density profile to 800 m depth was approximated by a simple model consisting of a mixed layer of constant density, a linear pycnocline between the mixed layer depth and a second depth marking the base of the pycnocline, and a pycnostad of a lesser density gradient beneath the base of the pycnocline. The five parameters of this pycnocline approximation were fit by an algorithm based on a downhill simplex method of minimization (AMOEBAS subroutine in Press et al., 1989). Pycnocline depth is the midpoint of the line segment approximating the pycnocline; pycnocline strength is the slope of this line segment. Pycnocline type is indexed by a ratio (PR) indicating the relative contribution of potential temperature (θ) and salinity (S) to the change in potential density (σ) between the standard depths above (1) and below (2) the pycnocline depth:

$$\text{PR} = [\Delta\sigma(\theta) - \Delta\sigma(S)]/\Delta\sigma(\theta, S)$$

Table 1

Statistics for gridding horizontal fields of hydrographic variables by loess-weighted least squares regression

Variable	N	n_{\min}	d_{\min} (d_{\max})	r^2
Surface temperature	550,307	3000	3 (8.2)	0.73–0.84
Surface salinity	166,949	5000	3 (15.0)	0.56–0.72
Thermocline depth	446,059	3000	3 (8.7)	0.47–0.63
Thermocline strength	442,077	3000	3 (8.7)	0.47–0.61
Mixed layer depth	441,180	3000	3 (8.7)	0.53–0.67
Surface phosphate	24,506	1000	5 (20)	0.60–0.78
Surface silicate	19,248	1000	5 (20)	0.54–0.68
Surface nitrate	16,386	1000	5 (20)	0.63–0.85
Oxygen minimum	11,998	1000	5 (20)	0.46–0.82

N = total number of WOD01 stations in study region with valid data, n_{\min} = minimum number of observations for grid point regression estimate (n_{\min} observations for nutrients and oxygen not always found within $d \leq 20$), d_{\min} = minimum search radius (equivalent to degrees latitude), r^2 = fraction of total variance explained (first to third quartiles of grid point values).

where $\Delta\sigma(\theta) = \sigma(\theta_2, S_1, P_2) - \sigma(\theta_1, S_1, P_1)$ is the change in density attributable to temperature and pressure, $\Delta\sigma(S) = \sigma(\theta_1, S_2, P_2) - \sigma(\theta_1, S_1, P_1)$ is the change in density attributable to salinity and pressure, and $\Delta\sigma(\theta, S) = \sigma(\theta_2, S_2, P_2) - \sigma(\theta_1, S_1, P_1)$ is the change in density attributable to temperature, salinity and pressure.

PR values < 0 indicate that the pycnocline stratification is primarily a halocline, values > 0 that the pycnocline is primarily a thermocline, and values > 1 that the thermocline is partially opposed by a reverse or destratifying halocline ($\Delta\sigma(S) < 0$). Note that PR values in the ranges of < 0 , $0-1$, and > 1 are analogous to Turner angle values of -45 to 0 , 0 to $+45$, and $+45$ to $+90$, respectively (Ruddick, 1983). However, this is not a strict equivalence because PR is calculated between discrete standard depths separated by 20 or more meters and the Turner angle, or the density gradient ratio of which it is a transform, is an index of stability of oceanic fine structure.

References

- Amador, J.A., Alfaro, E.J., Lizano, O.G., Magaña, V.O., 2006. Atmospheric forcing of the eastern tropical Pacific: a review. *Progress in Oceanography* 69 (2–4), 101–142.
- Ando, K., McPhaden, M.J., 1997. Variability of surface layer hydrography in the tropical Pacific Ocean. *Journal of Geophysical Research-Oceans* 102, 23,063–23,078.
- Benway, H.M., Mix, A.C., 2004. Oxygen isotopes, upper-ocean salinity, and precipitation sources in the eastern tropical Pacific. *Earth and Planetary Science Letters* 224, 493–507.
- Brandhorst, W., 1959. Nitrification and denitrification in the eastern tropical North Pacific. *Journal Conseil International pour l'Exploration de la Mer* 25, 3–20.
- Conkright, M.E., Antonov, J.I., Baranova, O., Boyer, T.P., Garcia, H.E., Gelfeld, R., Johnson, D., Locarnini, R.A., Murphy, P.P., O'Brien, T.D., Smolyar, I., Stephens, C., 2002a. World Ocean Database 2001. Volume 1: Introduction NOAA Atlas NESDIS 42. U.S. Government Printing Office, Washington, DC, 167 pp.
- Conkright, M.E., Locarnini, R.A., Garcia, H.E., O'Brien, T.D., Boyer, T.P., Stephens, C., Antonov, J.I., 2002b. World Ocean Atlas 2001: Objective Analyses, Data Statistics, and Figures, CD-ROM Documentation. National Oceanographic Data Center, Silver Spring, MD, 17 pp.
- Chavez, F.P., Service, S.K., Buttrey, S.E., 1996. Temperature–nitrate relationships in the central and eastern tropical Pacific. *Journal of Geophysical Research-Oceans* 101, 20,553–20,563.
- Cline, J.D., Richards, F.A., 1972. Oxygen deficient conditions and nitrate reduction in the eastern tropical North Pacific Ocean. *Limnology and Oceanography* 17, 885–900.
- Cronin, M.F., Kessler, W.S., 2002. Seasonal and interannual modulation of mixed layer variability at 0° , 110° W. *Deep-Sea Research I* 49, 1–17.
- da Silva, A.M., Young, C.C., Levitus, S., 1994. Atlas of surface marine data 1994, Volume 4: Anomalies of fresh water fluxes. NOAA Atlas NESDIS 9, 308 pp.
- Dai, A., Wigley, T.M.L., 2000. Global patterns of ENSO-induced precipitation. *Geophysical Research Letters* 27, 1283–1286.
- De Boyer Montégut, C., Madec, G., Fischer, A.S., Lazar, A., Iudicone, D., 2004. Mixed layer depth over the global ocean: an examination of profile data and a profile-based climatology. *Journal of Geophysical Research-Oceans* 109, C12003. doi:10.1029/2004JC002378.
- Delcroix, T., 1998. Observed surface oceanic and atmospheric variability in the tropical Pacific at seasonal and ENSO timescales: a tentative overview. *Journal of Geophysical Research-Oceans* 103, 18,611–18,633.
- Dore, J.E., Karl, D.M., 1996. Nitrite distributions and dynamics at station ALOHA. *Deep-Sea Research II* 43, 385–402.
- Fiedler, P.C., 2002. The annual cycle and biological effects of the Costa Rica Dome. *Deep-Sea Research I* 49, 321–338.
- Fiedler, P.C., Lavín, M., 2006. Introduction: a review of eastern tropical Pacific oceanography. *Progress in Oceanography* 69 (2–4), 94–100.
- Fine, R.A., Maillet, K.A., Sullivan, K.F., Willey, D., 2001. Circulation and ventilation flux of the Pacific Ocean. *Journal of Geophysical Research-Oceans* 106, 22,159–22,178.
- Fofonoff, N.P., 1985. Physical properties of seawater: a new salinity scale and equation of state for seawater. *Journal of Geophysical Research-Oceans* 90, 3332–3342.
- Hanawa, K., Talley, L.D., 2001. Mode waters. In: Siedler, G., Church, J., Gould, J. (Eds.), *Ocean Circulation and Climate: Observing and Modeling the Global Ocean*. Academic Press, New York, pp. 373–386.
- Hastenrath, S., 2002. The Intertropical Convergence Zone of the eastern Pacific revisited. *International Journal of Climatology* 22, 347–356.
- Hautala, S.L., Roemmich, D.H., 1998. Subtropical mode water in the Northeast Pacific Basin. *Journal of Geophysical Research-Oceans* 103, 13,055–13,066.
- Hayes, S.P., Toole, J.M., Mangum, L.J., 1983. Water-mass and transport variability at 110° W in the equatorial Pacific. *Journal of Physical Oceanography* 13, 153–168.
- Huang, R.-X., Qiu, B., 1998. The structure of the wind-driven circulation in the subtropical South Pacific Ocean. *Journal of Physical Oceanography* 28, 1173–1186.

- Jenkins, W.J., 1996. Tritium and ^3He in the WOCE Pacific Programme. *International WOCE Newsletter* 23, 6–9.
- Jiang, M.-S., Chai, F., Dugdale, R.C., Wilkerson, F.P., Peng, T.-H., Barber, R.T., 2003. A nitrate and silicate budget in the equatorial Pacific Ocean: a coupled physical–biological model study. *Deep-Sea Research II* 50, 2971–2996.
- Johnson, G.C., McPhaden, M.J., 1999. Interior pycnocline flow from the subtropical to the equatorial Pacific Ocean. *Journal of Physical Oceanography* 29, 3073–3089.
- Johnson, G.C., Moore, D.W., 1997. The Pacific subsurface countercurrents and an inertial model. *Journal of Physical Oceanography* 27, 2448–2459.
- Johnson, G.C., Toole, J.M., 1993. Flow of deep and bottom waters in the Pacific at 10°N . *Deep-Sea Research I* 40, 371–394.
- Johnson, G.C., Sloyan, B.M., Kessler, W.S., McTaggart, K.E., 2002. Direct measurements of upper ocean currents and water properties across the tropical Pacific during the 1990s. *Progress in Oceanography* 52, 31–61.
- Kamykowski, D., Zentara, S.J., 1986. Predicting plant nutrient concentrations from temperature and sigma-t in the upper kilometer of the world ocean. *Deep-Sea Research I* 33, 89–105.
- Kamykowski, D., Zentara, S.J., 1990. Hypoxia in the world ocean as recorded in the historical data set. *Deep-Sea Research I* 37, 1861–1874.
- Karl, D.M., 1999. A sea of change: biogeochemical variability in the North Pacific Subtropical Gyre. *Ecosystems* 2, 181–214.
- Kessler, W.S., 1990. Observations of long Rossby waves in the northern tropical Pacific. *Journal of Geophysical Research-Oceans* 95, 5183–5217.
- Kessler, W.S., 2006. The circulation of the eastern tropical Pacific: a review. *Progress in Oceanography* 69 (2–4), 181–217.
- Kester, D.R., 1975. Dissolved gases other than CO_2 , second ed.. In: Riley, J.P., Skirrow, G. (Eds.), *Chemical Oceanography*, vol. 1 Academic Press, New York, pp. 498–556.
- Laird, N.P., 1971. Panama Basin deep-water: properties and circulation. *Journal of Marine Research* 29, 226–234.
- Large, W.G., Nurser, A.J.G., 2001. Ocean surface water mass transformation. In: Siedler, G., Church, J., Gould, J. (Eds.), *Ocean Circulation and Climate: Observing and Modeling the Global Ocean*. Academic Press, New York, pp. 317–336.
- Lonsdale, P., 1976. Abyssal circulation of the southeastern Pacific and some geological implications. *Journal of Geophysical Research-Oceans* 81, 1163–1176.
- Lukas, R., 1986. The termination of the Equatorial Undercurrent in the eastern Pacific. *Progress in Oceanography* 16, 63–90.
- Lukas, R., Lindstrom, E., 1991. The mixed layer of the western equatorial Pacific Ocean. *Journal of Geophysical Research-Oceans* 96 (Suppl.), 3343–3357.
- Luyten, J., Pedlosky, P., Stommel, H., 1983. The ventilated thermocline. *Journal of Physical Oceanography* 13, 292–309.
- Marin, F., Hua, B.L., Wacongne, S., 2000. The equatorial thermocline and subsurface countercurrents in the light of the dynamics of atmospheric Hadley cells. *Journal of Marine Research* 58, 405–437.
- McCartney, M.S., 1982. The subtropical recirculation of Mode Waters. *Journal of Marine Research* 40 (Suppl.), 427–464.
- McPhaden, M.J., 1984. On the dynamics of equatorial subsurface countercurrents. *Journal of Physical Oceanography* 14, 1216–1225.
- Montgomery, R.B., Stroup, E.D., 1962. Equatorial waters and currents at 150°W in July–August 1952. *The Johns Hopkins Oceanographic Studies* 1, 68.
- O'Connor, B.M., Fine, R.A., Maillet, K.A., Olson, D.B., 2002. Formation rates of subtropical underwater in the Pacific Ocean. *Deep-Sea Research I* 49, 1571–1590.
- Östlund, H.G., Craig, H., Broecker, W.S., Spencer, D., 1987. *GEOSecs Atlantic, Pacific and Indian Ocean Expeditions; Shorebased Data and Graphics*, vol. 7. National Science Foundation, Washington, DC, 230 p.
- Pennington, J.T., Mahoney, K.L., Kuwahara, V.S., Kolber, D.D., Calienes, R., Chavez, F.P., 2006. Primary production in the eastern tropical Pacific: a review. *Progress in Oceanography* 69 (2–4), 285–317.
- Pickard, G.L., Emery, W.J., 1990. *Descriptive Physical Oceanography: An Introduction*, fifth ed. Pergamon Press, Oxford.
- Polovina, J.J., Mitchum, G.T., Evans, G.T., 1995. Decadal and basin-scale variation in mixed layer depth and the impact on biological production in the Central and North Pacific, 1960–88. *Deep-Sea Research* 42, 1701–1716.
- Press, W.H., Flannery, B.P., Teukolsky, S.A., Vetterling, W.T., 1989. *Numerical Recipes: The Scientific Art of Computing (FORTRAN Version)*. Cambridge University Press, Cambridge, 702 pp.
- Reid, J.L., 1973. The shallow salinity minima of the Pacific Ocean. *Deep-Sea Research I* 20, 51–68.
- Reid, J.L., 1981. On the mid-depth circulation of the world ocean. In: Warren, B.A., Wunsch, C. (Eds.), *Evolution of Physical Oceanography: Scientific Surveys in Honor of Henry Stommel*. MIT Press, Cambridge, pp. 70–111.
- Reid, J.L., 1997. On the total geostrophic circulation of the Pacific Ocean: flow patterns, tracers, and transports. *Progress in Oceanography* 39, 263–352.
- Richards, F.A., 1957. Oxygen in the ocean. *Geological Society of America Memoir* 67 (1), 185–238.
- Ridgeway, K.R., Dunn, J.R., Wilkin, J.L., 2002. Ocean interpolation by four-dimensional weighted least squares – application to the waters around Australia. *Journal of Oceanic and Atmospheric Technology* 19, 1357–1375.
- Riley, G.A., 1941. Oxygen, phosphate, and nitrate in the Atlantic Ocean. *Bulletin Bingham Oceanographic Collection* 13, 1–126.
- Rowe, G.D., Firing, E., Johnson, G.C., 2000. Pacific equatorial subsurface countercurrent velocity, transport, and potential vorticity. *Journal of Physical Oceanography* 30, 1172–1187.
- Ruddick, B., 1983. A practical indicator of the stability of the water column to double-diffusive activity. *Deep-Sea Research* 10, 1105–1107.
- Sarmiento, J.L., Herbert, T.D., Toggweiler, J.R., 1988. Causes of anoxia in the world ocean. *Global Biogeochemical Cycles* 2, 115–128.
- Schlitzer, R., 2002. *Ocean Data View*. Available from: <<http://www.awi-bremerhaven.de/GEO/ODV>>.
- Shea, D.J., Trenberth, K.E., Reynolds, W., 1992. A global monthly sea surface temperature climatology. *Journal of Climate* 5, 987–1001.

- Sloyan, B.M., Johnson, G.C., Kessler, W.S., 2003. The Pacific cold tongue: a pathway for interhemispheric exchange. *Journal of Physical Oceanography* 33, 1027–1043.
- Sparrow, M., Chapman, P., Gould, J. (eds.) 2005–2006. The World Ocean Circulation Experiment (WOCE) Hydrographic Programme Atlas Series (4 volumes), International WOCE Project Office, Southampton, UK.
- Sprintall, J., Tomczak, M., 1992. Evidence of the barrier layer in the surface layer of the tropics. *Journal of Geophysical Research-Oceans* 97, 7305–7316.
- Sverdrup, H.U., Johnson, M.W., Fleming, R.H., 1942. *The Oceans: Their Physics, Chemistry, and General Biology*. Prentice-Hall, Englewood Cliffs.
- Talley, L.D., 1993. Distribution and formation of North Pacific Intermediate Water. *Journal of Physical Oceanography* 23, 517–537.
- Talley, L.D., Johnson, G.C., 1994. Deep, zonal subequatorial flows. *Science* 263, 1125–1128.
- Thomas, W.H., 1966. On denitrification in the northeastern tropical Pacific Ocean. *Deep-Sea Research I* 13, 1109–1114.
- Tomczak, M., Godfrey, J.S., 2001. *Regional Oceanography: An Introduction*. Pdf version 1.2. Available from: <<http://www.es.flin-ders.edu.au/~mattom/regoc/pdfversion.html>>.
- Tsuchiya, M., 1968. Upper waters of the intertropical Pacific Ocean. *The Johns Hopkins Oceanographic Studies* 4, 50.
- Tsuchiya, M., 1981. The origin of the Pacific Equatorial 13 °C Water. *Journal of Physical Oceanography* 11, 794–812.
- Tsuchiya, M., Talley, L.D., 1996. Water-property distributions along an eastern Pacific hydrographic section at 135°W. *Journal of Marine Research* 54, 541–564.
- Tsuchiya, M., Talley, L.D., 1998. A Pacific hydrographic section at 88°W: water-property distribution. *Journal of Geophysical Research-Oceans* 103, 12,899–12,918.
- Tsuchiya, M., Lukas, R., Fine, R.A., Firing, E., Lindstrom, E., 1989. Source waters of the Pacific Equatorial Undercurrent. *Progress in Oceanography* 23, 101–147.
- Tyrell, T., Law, C.S., 1997. Low nitrate:phosphate ratios in the global ocean. *Nature* 387, 793–796.
- Wang, C., Enfield, D.B., 2001. The tropical Western Hemisphere warm pool. *Geophysical Research Letters* 28, 1635–1638.
- Wang, C., Fiedler, P.C., 2006. ENSO variability in the eastern tropical Pacific: a review. *Progress in Oceanography* 69 (2–4), 239–266.
- Wang, B., Wu, R., Lukas, R., 2000. Annual adjustment of the thermocline in the tropical Pacific Ocean. *Journal of Climate* 13, 596–616.
- Weiss, R.F., 1970. The solubility of nitrogen, oxygen and argon in water and seawater. *Deep-Sea Research* 17, 721–735.
- Wijffels, S.E., Toole, J.M., Bryden, H.L., Fine, R.A., Jenkins, W.J., Bullister, J.L., 1996. The water masses and circulation at 10°N in the Pacific. *Deep-Sea Research* 43, 501–544.
- Willett, C.S., Leben, R., Lavín, M.F., 2006. Eddies and mesoscale processes in the eastern tropical Pacific: a review. *Progress in Oceanography* 69 (2–4), 218–238.
- Wong, A.P.S., Johnson, G.C., 2003. South Pacific eastern subtropical mode water. *Journal of Physical Oceanography* 33, 1493–1509.
- Wooster, W., Cromwell, T., 1958. An oceanic description of the eastern equatorial Pacific. *Scripps Institution Oceanographic Bulletin* 7, 169–282.
- Wyrtki, K., 1962. The oxygen minima in relation to ocean circulation. *Deep-Sea Research* 9, 11–23.
- Wyrtki, K., 1964a. Upwelling in the Costa Rica Dome. *Fishery Bulletin* 63, 355–372.
- Wyrtki, K., 1964b. The thermal structure of the eastern Pacific Ocean. *Deutschen Hydrographischen Zeitschrift, Ergänzungsheft A* 6, 84.
- Wyrtki, K., 1966. Oceanography of the eastern equatorial Pacific Ocean. *Oceanography and Marine Biology Annual Review* 4, 33–68.
- Wyrtki, K., 1967. Circulation and water masses in the eastern equatorial Pacific Ocean. *International Journal of Oceanology and Limnology* 1, 117–147.
- Wyrtki, K., 1975a. Fluctuations of the dynamic topography in the Pacific Ocean. *Journal of Physical Oceanography* 5, 450–459.
- Wyrtki, K., 1975b. El Niño – the dynamic response of the equatorial Pacific Ocean to atmospheric forcing. *Journal of Physical Oceanography* 5, 572–584.
- Wyrtki, K., 1981. An estimate of equatorial upwelling in the Pacific. *Journal of Physical Oceanography* 11, 1205–1214.
- Wyrtki, K., Kilonsky, B., 1984. Mean water and current structure during the Hawaii-to-Tahiti Shuttle Experiment. *Journal of Physical Oceanography* 14, 242–263.
- Xie, P., Arkin, P.A., 1997. Global precipitation: a 17-year monthly analysis based on gauge observations, satellite estimates, and numerical model outputs. *Bulletin American Meteorological Society* 78, 2539–2558.
- You, Y., 2003. The pathway and circulation of North Pacific Intermediate Water. *Geophysical Research Letters* 30, 2291. doi:10.1029/2003GL018561.
- Yuan, X., Talley, L.D., 1992. Shallow salinity minima in the North Pacific. *Journal of Physical Oceanography* 22, 1302–1316.
- Zentara, S.J., Kamykowski, D., 1977. Latitudinal relationships among temperature and selected plant nutrients along the west coast of North and South America. *Journal of Marine Research* 35, 321–337.